Rivista Italiana di Paleontologia e Stratigrafia
(*Research in Paleontology and Stratigraphy*)
vol. 131(1): 139-175. **March 2025**
DOI: https://doi.org/10.54103/2039-4942/22338

A NEW PLIOCENE SPERM WHALE FROM VIGLIANO D'ASTI, PIEDMONT, NORTHWEST ITALY

MICHELANGELO BISCONTI[1,2,*], RICCARDO DANIELLO[1], RICCARDO STECCA[1] & GIORGIO CARNEVALE[1]

[1]Dipartimento di Scienze della Terra, Università degli Studi di Torino, via Valperga Caluso 35, 10100, Torino.
E-mail: michelangelo.bisconti@unito.it; riccardo.daniello@edu.unito.it; riccardo.stecca@edu.unito.it; giorgio.carnevale@unito.it.
[2]San Diego Natural History Museum, 1788 El Prado, San Diego, CA 92102, USA.
*Corresponding author.

Associate Editor: Lars Werdelin.

To cite this article: Bisconti M., Daniello R., Stecca R. & Carnevale G. (2025) - A new Pliocene sperm whale from Vigliano D'Asti, Piedmont, Northwest Italy. *Rivista Italiana di Paleontologia e Stratigrafia,* 131(1): 139-175.

Keywords: Italy; Physeteridae; Phylogeny; *Eophyseter*; Physeteroidea; Piedmont; Pliocene; Postcranial skeleton.

Abstract. A new sperm whale species is described from the late Zanclean (Early Pliocene) of Piedmont, northwest Italy, based on a partial vertebral column and parts of the forelimb. The new taxon, *Eophyseter damarcoi* gen. nov. sp. nov., is characterized by elongated vertebral centra in the thoracic and lumbar regions of the vertebral column, wider and higher articular facets for the occipital condyles in the atlas, elliptical and dorsoventrally compressed posterior articular facet of the axis-bearing block, ulna with posteriorly convex margin. These characters distinguish *Eophyseter damarcoi* gen. nov. sp. nov. from other physeteroids and show that the vertebral proportions are differently arranged with respect to those of the extant sperm whale species. A phylogenetic analysis was performed to understand the relationships of *Eophyseter damarcoi* gen. nov. sp. nov. by adding 20 postcranial characters to a previous character x taxon matrix; it revealed that *E. damarcoi* gen. nov. sp. nov. forms a clade with *P. macrocephalus*. A taphonomic analysis suggested that the carcass of the holotype specimen of *Eophyseter damarcoi* gen. nov. sp. nov. was exploited by sharks and colonized by barnacles and molluscs; however, a quick burial prevented its total destruction by other invertebrates, as usual in the cetacean fossil record from the Pliocene of Piedmont.

Introduction

In the last days of November 1929 a skeleton of a sperm whale was found in the Pliocene outcrop of the Sabbie d'Asti Formation near Valmontasca village in the municipality of Vigliano d'Asti (about 4 km South of Asti and about 45 km South-East of Torino, Piedmont, North-West Italy; Fig. 1). A living witness of the excavation has recently reported that the skeleton was perfectly articulated and headless, and it seemed a sea snake (Nosenzo 2022). The specimen was excavated during the 1929 winter and was transported to Torino in January 1930 where it was consolidated. A preliminary report on this sperm whale was published by Parona (1930) who described the excavation and the consolidation procedures, and who provided a first taxonomic assessment based on the morphology of the vertebral column. This early account was supported by Richard (1930) who took

Received: January 22, 2024; accepted: January 16, 2025

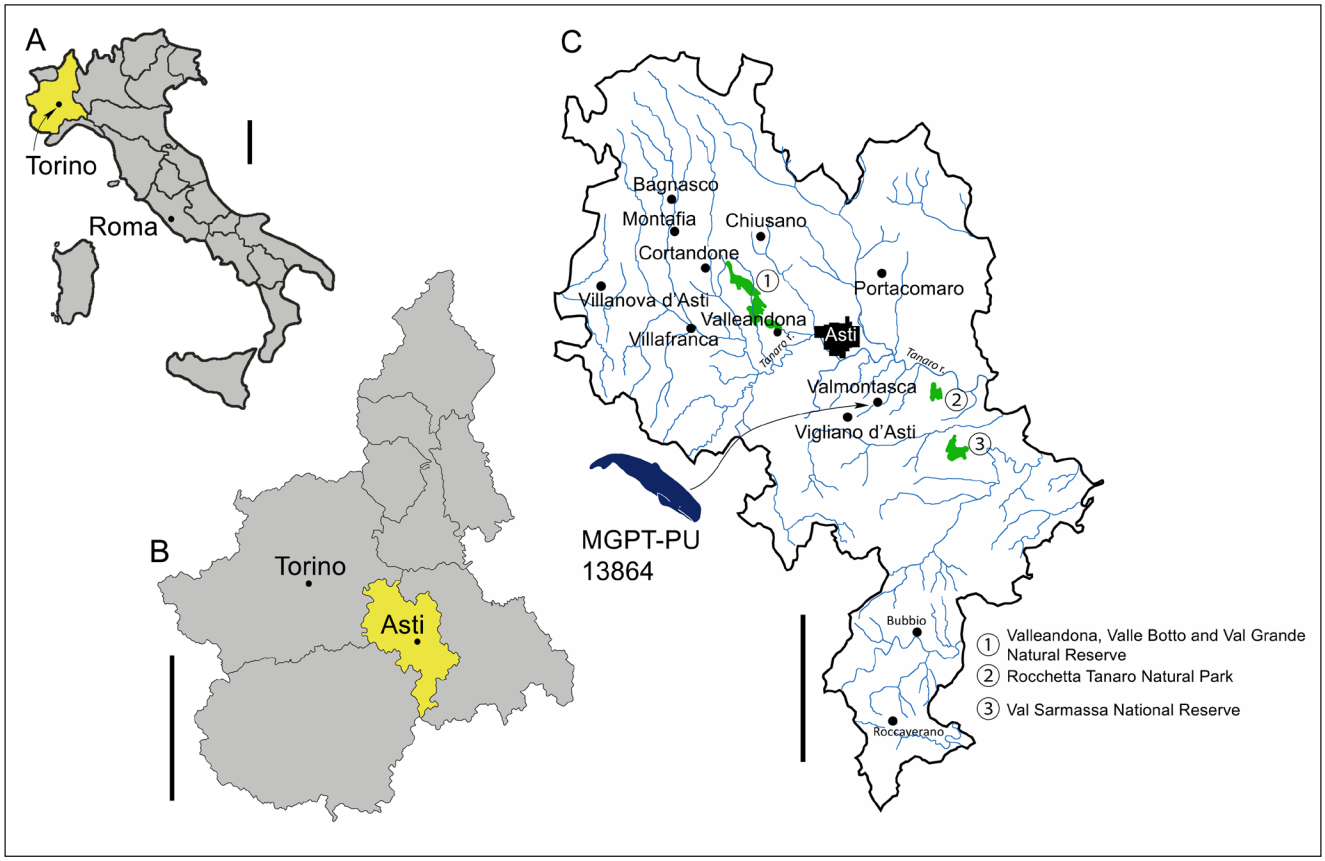

Fig. 1 - Location of the discovery of MGPT-PU 13864, holotype of *Eophyseter damarcoi* gen. nov. sp. nov. A) Map showing the Italian peninsula with Piedmont indicated in yellow; scale bar equals 100 km. B) Map of Piedmont showing the extension of the Asti province; scale bar equals 50 km. C) Map showing the Asti province with indication of the locality of the discovery of MGPT-PU 13864; scale bar equals 20 km.

the responsibility for the preparation and consolidation of the specimen together with its anatomical study. Both Parona and Richard concluded that the specimen represented a Pliocene sperm whale close to the extant sperm whale species, *Physeter macrocephalus* Linnaeus, 1758. They further suggested that, based on the asymmetry observed in one chevron bone, this Pliocene sperm whale was particularly close to the southern population of *P. macrocephalus* that, at that time, was assigned to its own species, *Physeter australis* Gray, 1846. Socin (1954) briefly reviewed this find and assigned it to *Physeter australis* var. *astensis* following Sacco's philosophy about the use of varieties in the systematics of fossil cetaceans (Sacco 1897, 1899; see also Bisconti et al. 2020, 2021 for historical studies).

After about one century, the specimen was newly prepared for an exhibition at the Museo Paleontologico Territoriale dell'Astigiano (hereinafter: MPTA; Fig. 2A); this exhibition is part of broader scientific education programs carried out by this agency in the last ten years (Damarco et al. 2023; Bisconti et al. 2020, 2023a). During the new preparation process, the specimen was newly available for study allowing the realization of a MS thesis on the morphology of selected anatomical structures including the atlas, the scapula and the humerus that confirmed its close affinity with the living *Physeter macrocephalus* (Stecca 2021). However, further investigations on the vertebral characteristics revealed significant differences suggesting that the Vigliano sperm whale represents a new genus and species.

In this paper, we provide a detailed morphological study of the skeleton of the Vigliano sperm whale in a broader comparative context that includes extant and extinct physeteroid cetaceans. By means of this comparative analysis, we find that the Vigliano sperm whale represents a new taxon, *Eophyseter damarcoi* n. gen. and n. sp. that we define and dedicate to Piero Damarco, Paleontology curator at the Museo Paleontologico Territoriale dell'Astigiano (see below, Systematic Paleontology

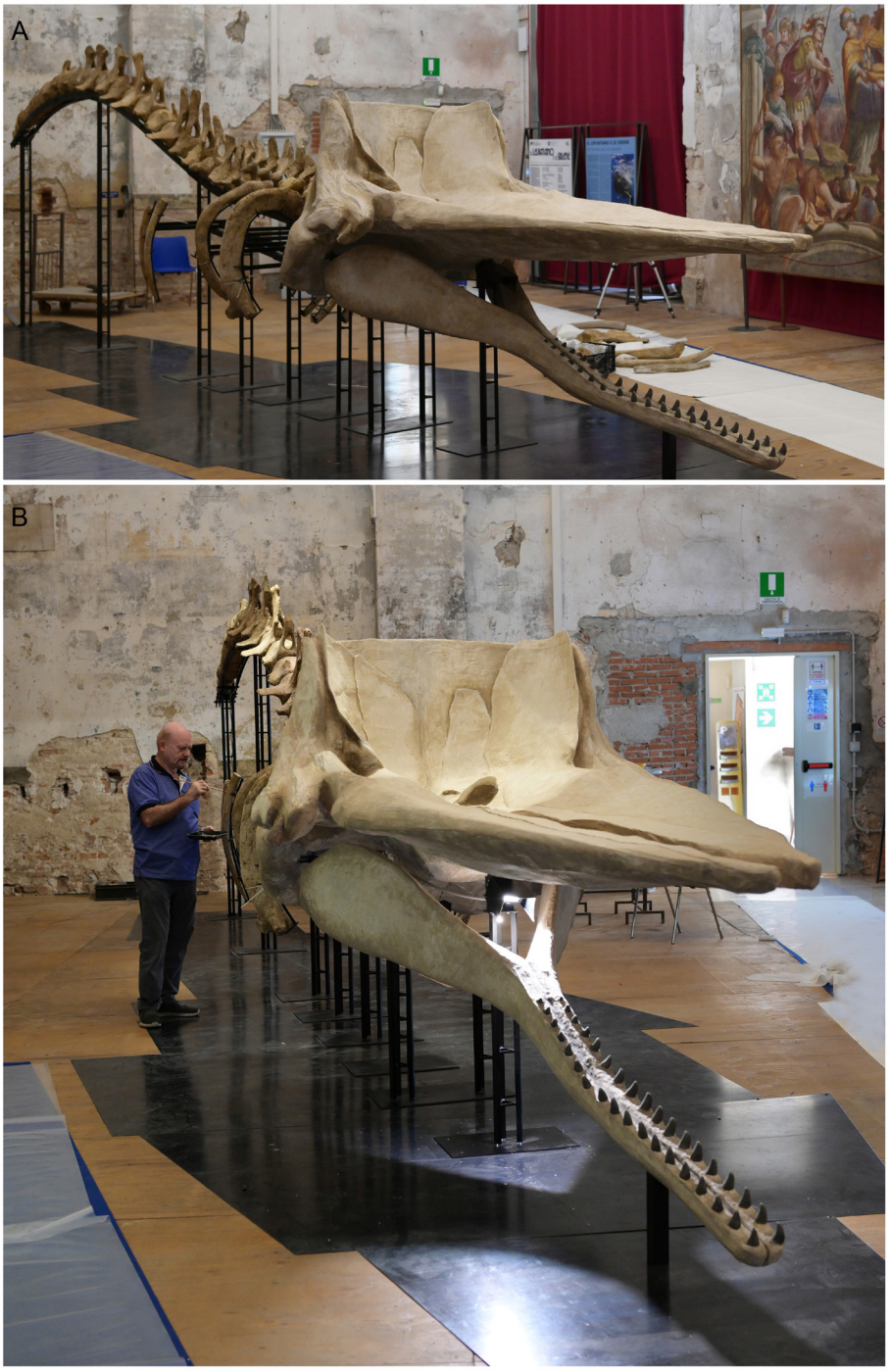

Fig. 2 - Reconstruction of the sperm whale *Eophyseter damarcoi* gen. nov sp. nov. (MGPT-PU 13864, holotype). A) Final preparation of the display in the Chiesa del Gesù, Michelerio Palace, Asti; note that the skull and the mandible are reconstructed based on their morphology in the modern sperm whale *Physeter macrocephalus*; a number of ribs is still to be mounted and is located on the ground on the left side of the skeleton. B) Piero Damarco, to whom *Eophyseter damarcoi* gen. nov. sp. nov. is dedicated, applying the final touch to the skeleton MGPT-PU 13864 on display in Asti.

section; Fig. 2B). Moreover, we assess the phylogenetic relationships of the Vigliano sperm whale by means of a cladistic analysis of Physeteroidea. Finally, we provide an assessment of the functional regionalization of the vertebral column of the Vigliano sperm whale that supports the definition of the new genus and species and sheds light on a scarcely understood aspect of the sperm whale evolutionary history, that is the evolution of the postcranial skeleton.

Material and methods

Studied specimen

This paper focuses on a partial skeleton from the Pliocene outcrop of the Sabbie d'Asti Formation near Vigliano d'Asti (Valmontasca village). The specimen is part of the collection of the Geological and Paleontological Museum of the University of Torino (hereinafter: MGPT) and is unambiguously identified by the number MGPT-PU 13864.

It is currently on exhibition at the Museo Paleontologico Territoriale dell'Astigiano in Asti (Fig. 2A). It consists of seven cervical vertebrae in two blocks, eleven thoracics, six lumbars and twelve caudal vertebrae (total: 36 vertebrae); seven ribs from the right side and eight ribs of the left side; partial sternum; left scapula, left humerus, partial radius and ulna, and three chevron. Skull, ear bones, mandible and teeth are absent.

Anatomical terminology, photography and measurements

Given that the skull is absent, we used the anatomical terminology for postcranial skeleton provided by Bisconti & Carnevale (2022), Martínez-Cáceres et al. (2017) and Benke (1987). The specimen was photographed with a Nikon Z7 full frame mirrorless camera with Nikkor 24-70 mm f/4 and 40 mm f/2 lenses with a SB700 speedlight flash mounted on the camera. Pictures were adjusted in Adobe Photoshop 2023 and Nik Collection Viveza 3 for contrast, noise, sharpness and light. Measurements were taken with Sourcingmap (300 mm) and Tacklife D02 (150 mm) digital calipers with error margin to the nearest 0.1 mm.

Photogrammetry

For this project, we decided to 3D scan the whole skeleton, thus providing a complete 3D replica of the specimen. We started by performing photogrammetry of the vertebral column, taking pictures of the vertebrae using a Samsung a52s 64MP camera. The bones were photographed in groups of two or three on a single surface although some of them, like the atlas, have been individually photographed to obtain the maximum fidelity or due to issues with the reconstruction procedure.

On average, we acquired 190 photos per group which were then imported into Meshroom. The raw mesh from Meshroom was refined in Blender where we isolated each bone and fixed artifacts and meshes' topology. After we decimated the mesh and scaled the bones accordingly, we obtained a model made, on average, of 7100 polygons per vertebra and a total of 205792 polygons for the vertebral column.

The ribcage and forelimb were reconstructed subsequently. We acquired 260 pictures of both after the skeleton was mounted on its metal frame for the museum exhibition. The metal structure did not cause any major issues with the reconstruction in Meshroom. Once completed, it was manually removed in Blender while also applying the same procedure used with the vertebrae. This second model resulted in a 60510 polygon mesh, which was joined with the previously made model of the vertebral column.

For museum exhibition, we then added the cranium of a *Physeter macrocephalus* published by the Natural History Museum of London on Sketchfab (NHMUK ZD 2007.100, https://sketchfab.com/3d-models/sperm-whale-cranium-fcbaddea99a3408fbf2142556e84feb2) and the lower jaw from California Academy of Sciences of San Francisco also from Sketchfab (https://sketchfab.com/3d-models/sperm-whales-lower-jaw-cachalot-99770bded0ff43939de039a88ebc4f68) which were properly scaled to fit the atlas and complete the model, reproducing how the specimen is currently exhibited to the public in the museum.

An excerpt of the photogrammetry is shown in Fig. 3 including some views. The photogrammetry of MGPT-PU 13864 can be freely downloaded from Morphosource at the following link: n2t.net/ark:/87602/m4/598404.

Inference of body size

We are not aware of any statistical method able to infer the body size (skeletal length, total body length, body weight) from skeletal portions other than the skull for sperm whales. For this reason, we analyzed published data to find correlations between the size of specific postcranial bones and body size. In particular, Flower (1868) published the measurements of four sperm whales from the southern hemisphere (units were feet and inches) as reported in Table 1; he reported the measurements of the skull, the skeleton and the total body length of the intact animal. From his measurements it is clear that the skull represents a mean of 33.48% of the total skeletal length (the skull length/skeletal length ratio ranges from 28.54 to 39.03% in the four specimens). Flower (1868) published the measurements of the whole forelimb (corresponding to 11% of the total skeletal length), the height of the scapula and the proximodistal length of the humerus (Table 1) which we selected for a search of a relationship to the total body length. We calculated four ordinary least squares regression analyses by using Past (Hammer et al. 2001) and we found

Individual	SL (feet)[1]	SL (m)[1]	SkeL (feet)[1]	SkeL (m)[1]	LintA (feet)[1]	LintA (m)[1]	hSca (inches)[1]	hSca (m)[1]	LHum (inches)[1]	LHum (m)[1]	WC_1 (inches)[1]	WC_1 (m)[1]
1	16'9''	5.08	50'1''	15.26	60'	18.3	32 ½''	0.825	19 ¼''	0.488	37 ½''	0.95
2	17'9''	5.4	50'	15.24			36''	0.91	22 ¾''	0.578	36''	0.91
3	18'11''	5.75	48'4''	14.73			34''	0.86	18 1/4''	0.46		
4	16'	4.87	56'	17.06			35''	0.889	20''			

Tab. 1 - Measurements of the sperm whales published by Flower (1864). [1]Legend: SL, skull length; SkeL, skeletal length; LintA, length of intact animal; hSca, proximodistal height of scapula; LHum, proximodistal height of humerus; WC_1, width of atlas.

that all the points of the regression plots fall within the 95% confidence interval for the searched relationships. The search for the relationship between height of scapula and skull length resulted in the following equation (1):

Skull length = 0.32582 (height of scapula in m) + 4.9912

The search for the relationship between height of scapula and skeletal length resulted in the following equation (2):

Skeletal length = 9.1744 (height of scapula in m) + 7.5816

The same searches performed by including proximodistal length of humerus and skull and skeletal lengths provided the following equations (3) and (4):

Skull length = –1.3706 (length of humerus) + 6.1072

Skeletal length = 3.2106 (length of humerus) + 13.444

It must be taken in mind that these equations are based on an extremely limited number of individuals (Table 1) and that the species we are studying is different from those sampled in Table 1; for these reasons, the results are to be considered as mere approximations in the hope that future works will provide new measurements of sperm whale skeletons.

We then looked for eventual correlations among skeletal length and the total body length of the intact animal and found the intact animal is longer than its skeleton by about 15%, an amount that corresponds to the total intervertebral space. We applied equations (1)-to-(4) to evaluate the total skull length and the total skeletal length of MG-PT-PU 13864 and then corrected the total skeletal length by increasing it by 15%.

Functional regionalization of the vertebral column

Buchholtz (1998) provided a rationale to functionally interpret the morphometric variations measured in the vertebral centra of cetacean species. She demonstrated that length, width and height of vertebral centra can be used to graphically individuate different functional regions of the cetacean vertebral column that do not necessarily correspond to anatomical regions. Whereas it is common practice to distinguish between cervical, thoracic, lumbar and caudal vertebrae when describing a cetacean skeleton, it is not similarly common to find analyses of functional regionalization of the vertebral columns. Buchholtz (2004, 2005) studied the functional regionalization of the vertebral columns of Delphinidae and also detailed the swimming abilities of *Lagenorhynchus* Gray, 1846 by including additional metrics to her method. Moreover, she applied the method to fossil cetaceans including archaeocetes and mysticetes providing hypotheses about the swimming abilities of extinct whale species (Buchholtz 1998, 2001).

Variations in the morphometry of the vertebral centra may be shown in plots of length, width and height values for the whole vertebral column. Peaks in variations between adjacent vertebrae individuate boundaries of functional regions. Usually, in modern cetaceans, four functional regions are found by this method: (1) cervical (corresponding to cervical vertebrae), (2) chest (corresponding to part of the thoracic vertebrae), (3) torso (corresponding to part of the thoracic, the whole lumbar and anterior part of the caudal vertebrae), (5) peduncle and (6) fluke (corresponding to specific portions of the caudal section of the vertebral column. The relative extent of the different functional regions was correlated to different ways extant cetacean species undulate and oscillate their vertebral column during swimming (Buchholtz 2001). She found four fundamental movement patterns of the column in extant cetaceans and related these patterns to different patterns of functional regionalization of the vertebral columns. The main point of this method is that different morphometric patterns in the vertebral centra correspond to different functional re-

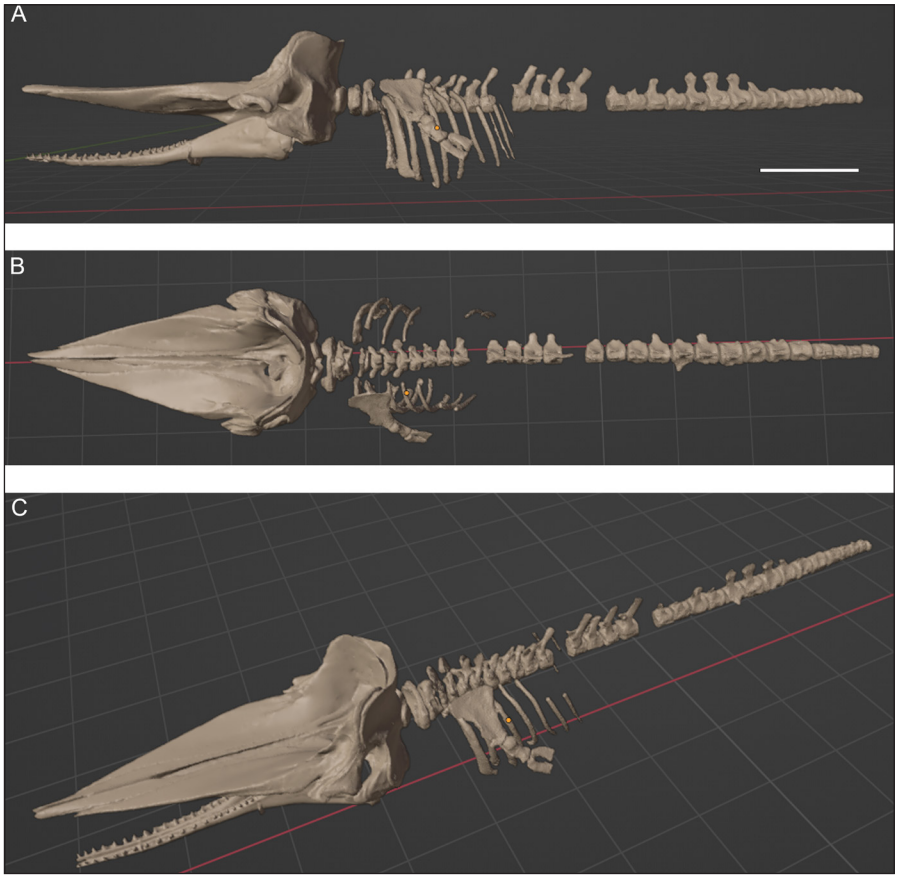

Fig. 3 - Excerpts from the photogrammetry of MGPT-PU 13864, holotype of *Eophyseter damarcoi* gen. nov. sp. nov. A) Lateral view. B) Dorsal view. C) Left dorsolateral view. Note that in the photogrammetry the reconstructed skull is also included that is not part of the original skeleton.

gionalizations of the vertebral columns which, in turn, correspond to different swimming behaviors.

Application of this method to the cetacean fossil record has been limited because of obvious problems due to the common incompleteness of postcranial skeletons. An attempt to use this method to characterize a Pliocene balaenid with peculiar vertebral and rib characters was done by Bisconti et al. (2023b) resulting in the inference of a different swimming behavior in the fossil species to extant right and bowhead species. We applied the Buchholtz (1998) method to MGPT-PU 13864 in order to provide biometric comparisons against the extant sperm whale *Physeter macrocephalus* and to characterize the functional regionalization of the vertebral column of the fossil specimen under investigation. We measured length, width and height of the vertebral centra and provide the resulting plots for both the extant sperm whale (data from Omura et al. 1962) and MGPT-PU 13864. Moreover, to better characterize morphometric patterns, we calculated the following parameters (from Buchholtz 1998, 2001, 2004, 2005): (1) relative centrum length (hereinafter: RCL), (2) percent change (hereinafter: PCH), (3) (centrum height/centrum width) ratio (hereinafter: CH/CW) and (4) 2CL/(CW+CH) which represents an averaged metric giving a summary view of dimensional changing along the vertebral column (hereinafter: SUM). Once all the biometric data were computed, we looked for possible correlations with the categories of swimming behaviors provided by Buchholtz (2001) and searched for similarities and differences in the functional patterns of the extant sperm whale and MGPT-PU 13864.

Phylogenetic analysis

We used the morphological dataset of Lambert et al. (2023) that was based on Peri et al. (2022), Alfsen et al. (2021) and Lambert et al. (2017). We accepted all the changes introduced in this dataset by Lambert et al. (2023) and added 20 characters from the postcranial skeleton. This is the first time that such an amount of postcranial data was added to a morphological analysis of the physeteroid phylogeny and for this reason, we provide descriptions for each of the characters together with a brief discussion in Supplementary Information Text S1. In total, the dataset used in the present paper includes 79 character states. The operational taxonomic units used here are 36, including MGPT-PU 13864 and

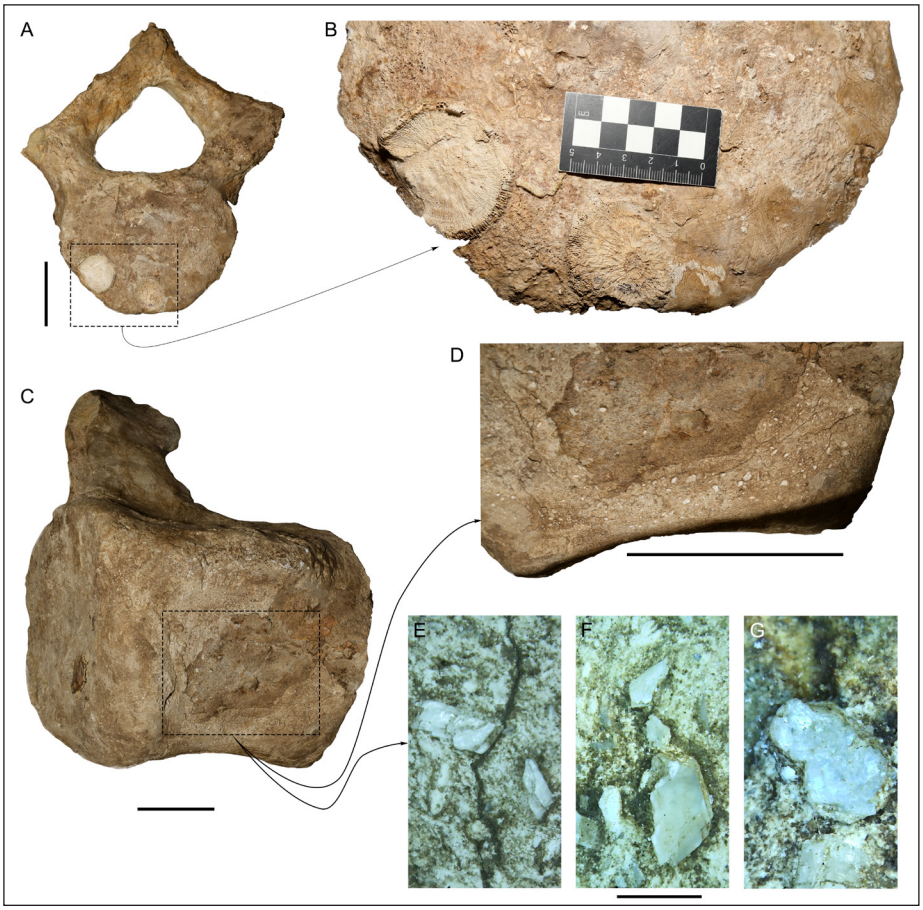

Fig. 4 - Taphonomy of MGPT-PU 13864. A) Third thoracic vertebra showing remains of two barnacles (in the dashed rectangle); scale bar equals 5 cm. B) Close-up view of the barnacles. C) Third lumbar vertebra with nacreous fragments; scale bar equals 5 cm. D) Close-up view of the nacreous fragments; scale bar equals 5 cm. E, F, G) Digital microscopy of the nacreous fragments; scale bar equals 1 mm.

four skeletons assigned to the extant *Physeter macrocephalus*. We included these four specimens to represent the individual variation observed in different skeletal districts by previous authors including Flower (1868), Omura et al. (1962), Van Beneden & Gervais (1880) and our own observations on the specimen MSNUP 265 currently on display at the Museo di Storia Naturale del Mediterraneo, Livorno (Roselli et al. 2014). The outgroup comparison criterion was used to determine the polarity of the character states and polarizations are explained on a character-by-character basis in Supplementary Information Text S1. The character x taxon matrix is shown in Supplementary Information Table S1.

We analyzed the matrix with TNT 1.5 (Goloboff & Catalano 2016) by using the Traditional search option that uses the tree bisection reconnection (TBR) algorithm with 10 trees to save per replication and 10 replicates with later archaeocetes as outgroups. We then performed a standard Bootstrap analysis (1000 replicates, Traditional Search, default parameter values). Both consistency and retention indices (respectively, CI and RI) were calculated through TNT; the homoplasy index (HI) was calculated by hand with the formula HI = 1 – CI. We studied the distribution of character states at ancestral nodes by using Mesquite 3.61 (Maddison & Maddison 2019) by using the maximum likelihood (ML) algorithm with the default Mk1 model.

Taphonomy

The completeness of the skeleton may be visually assessed in Supplementary Information Fig. S1 that is based on the skeletal components of the extant sperm whale (Flower 1868; Omura et al. 1962). Assuming that the number of the bones of MGPT-PU 13864 was the same as that of the extant sperm whale (that is, 133 assuming that the head can be dismembered in five different components including skull, right and left dentaries, right and left tympanoperiotic bones), the overall completeness of the Pliocene sperm whale from Vigliano is 41.3%.

The specimen was found in articulation (Parona 1930; Richard 1930) but in the early reports there are no maps of bone dispersion. The state-

Vertebra[1]	Neural arch	Neural apophysys	Right transverse process	Left transverse process	Shape of transverse process	Basis of transverse process	Ventral keel	Attachments for chevron	Foramen at base of transverse process	
									Right side	Left side
C_1	complete	absent	complete	complete						
C_2-C_7	complete	eroded	complete	complete						
T_1	complete	incomplete	complete	complete	tubercle	neural arch				
T_2	complete	complete	complete	complete	tubercle	neural arch				
T_3	complete	incomplete	-	-	tubercle	neural arch				
T_4	complete	complete	complete	complete	tubercle	neural arch				
T_5	complete	complete	complete	complete	tubercle	neural arch				
T_6	complete	incomplete	incomplete	-	tubercle	upper half				
T_7	complete	incomplete	-	-	tubercle	neural arch				
T_8	complete	incomplete	incomplete	-	flat	mid-height	?			
T_9	complete	incomplete	incomplete	-	flat	mid-height	Yes			
T_{10}	complete	complete	incomplete	-	?flat	upper half	-			
T_{11}	complete	complete	-	incomplete	?	mid-height	Yes			
L_1	Incomplete	-	-	-	tubercle	mid-height	Yes			
L_2	complete	complete	complete	-	?	upper half	Yes			
L_3	complete	incomplete	-	-	flat, long	mid-height	Yes			
L_4	complete	complete	complete	-	flat, long	mid-height	Yes	posterior		
L_5	incomplete	incomplete	incomplete	incomplete	flat, long	mid-height	-	-		
L_6	complete	incomplete	incomplete	-	flat, long	mid-height	-	-		
Ca_1	complete	complete	complete	-	flat, long	upper half	-	posterior		
Ca_2	complete	complete	incomplete	-	?	mid-height	-	yes		
Ca_3	complete	complete	-	-	blade-like	mid-height		yes		
Ca_4	-	-	complete	complete	?	mid-height		yes	complete	complete
Ca_5	incomplete	-	-	-	blade-like	mid-height		yes	incomplete	incomplete
Ca_6	complete	complete	complete	complete	-	-		yes	complete	complete
Ca_7	-	-	-	-	-	-		yes	complete	complete
Ca_8	complete	complete	-	-	-	-		yes	complete	complete
Ca_9	complete	complete	-	-	-	-		yes	complete	complete
Ca_{10}	No neural canal		-	-	-	-			complete	complete
Ca_{11}			-	-	-	-				
Ca_{12}			-	-	-	-				

Tab 2 - Preservation and morphology of the vertebral column of MGPT-PU 13864, holotype of *Eophyseter damarcoi* gen. nov. sp. nov. Caption: - not preserved; ?poorly preserved and impossible to describe.

ment that, at the time of the discovery, the specimen was found in anatomical articulation is consistent with the presence of almost all the neural processes of the vertebrae and of most of the vertebral column. The transverse processes are preserved on the right sides of the vertebrae but those from the left side are mainly lost (17 processes are completely or incompletely preserved on the right side and only 10 from the left side; Table 2). This observation suggests that the carcass was lying on the right flank at the time of its deposit on the sea floor. After the decay of the soft tissues, the right sides of the vertebrae were immersed in soft sediment and for this reason most of the transverse processes of the right side are now preserved. The transverse processes of the left side were exposed for longer time and suffered more from physical degradation and, in the end, most of them were lost. The permanence of most of transverse and neural processes in the fossil vertebral column is an indication that these bones were not subject to movement over the sea floor and, indirectly, that the vertebral column was not significantly dismembered and the vertebrae were not displaced after the decay of the soft tissues (Liebig et al. 2003). Such an indication supports the report that the skeleton was fully articulated in the early literature and by a living witness (Nosenzo 2022). The lack of the skull, both mandibular rami and parts of the forelimbs suggest that the carcass floated for a while before being deposited on the sea floor (Boessenecker 2013).

There are barnacle remains on the third thoracic vertebra (transverse diameter ranges from 48 to 50 mm; Fig. 4A, B). Shell fragments are observed on the third lumbar vertebra (Fig 4C-E) and barnacle traces are present on one rib (Fig 5). Shark bite marks are observed on the first right rib (Fig. 6) that show sharp, linear margins thus excluding that they were made by a white shark or any other shark with serrated teeth (Fig. 6C-E). In general, the microstructures of the bones are well-preserved and trabeculae and lacunae can be easily appreciated in the natural cross-sections of the bones (Fig. 7). In

Fig. 5 - Taphonomy of MGPT-PU 13864. A) Proximal portion of a rib (*m* in Fig. 13) showing traces of barnacle attachments in the dashed rectangle; scale bar equals 5 cm. B) Close-up view of the proximal portion with indicated the best preserved barnacle attachment scar (dashed rectangle). C) Digital microscopy of the barnacle attachment scar indicated in the dashed rectangle in B; scale bar equals 1 mm.

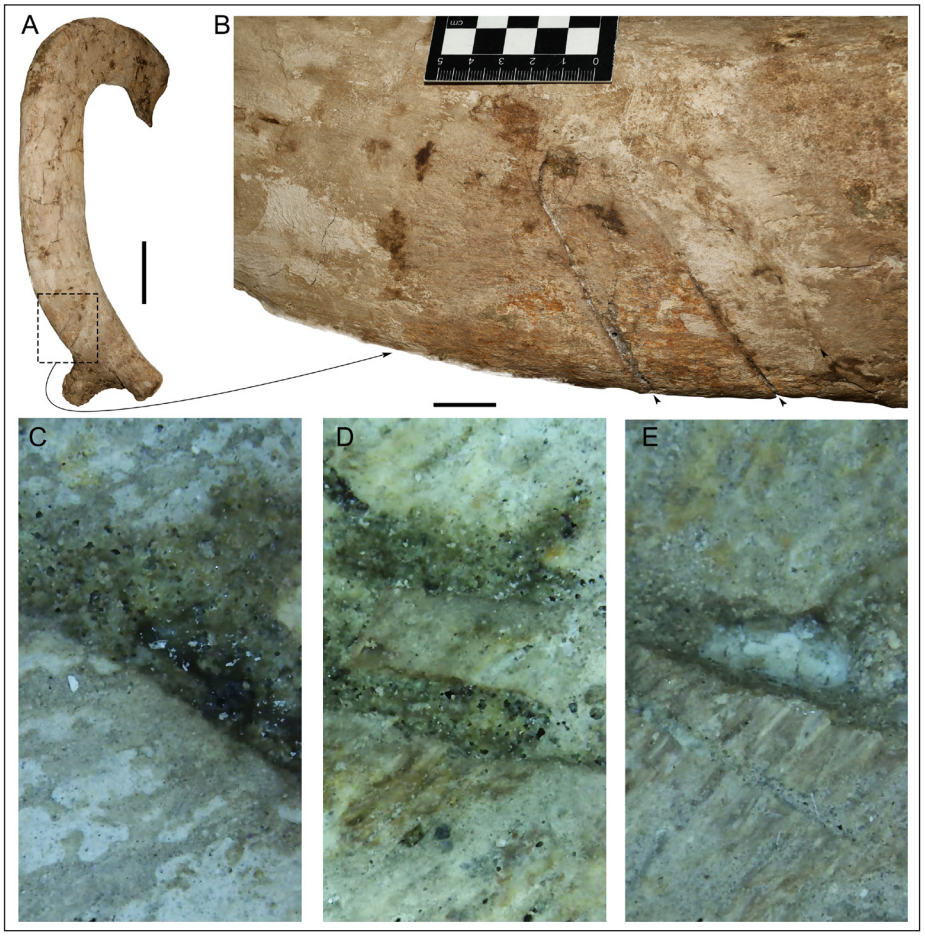

Fig. 6 - Taphonomy of MGPT-PU 13864. A) First left rib showing shark's bite marks in the dashed rectangle; scale bar equals 10 cm. B) Close-up view of the shark's bite marks indicated by the arrowheads. C, D, E) Digital microscopy of portions of the shark's bite marks showing sharp borders; scale bar equals 1 mm.

some cases, the sediment entered the lacunae and filled them so that the shape and volume of the lacunae is preserved even when the bony trabeculae are lost due to taphonomic processes (Fig. 7A, B).

The presence of both shark bite marks and barnacle traces suggests that the skeleton was not quickly buried once deposited on the sea floor. Rather, it remained on the sea floor for a period sufficient to allow the barnacles to grow on the bones (probably, for some months based on the diameter of the barnacle marks). The shark's bite marks suggest that the carcass was exploited before burial. In any case, the burial did not occur very long after the decay of most of the soft tissues because otherwise the skeleton would be heavily damaged by bioturbation, anatomical articulation would be lost and more dispersion of the bones would be noticed. An alternative explanation of the high quality preservation could be that the carcass was deposited in an anoxic floor but this is inconsistent with the presence of full-grown barnacles on the bones supporting the idea that this whale was deposited in a well-oxygenated sea floor. Another alternative explanation of the good preservation could be that

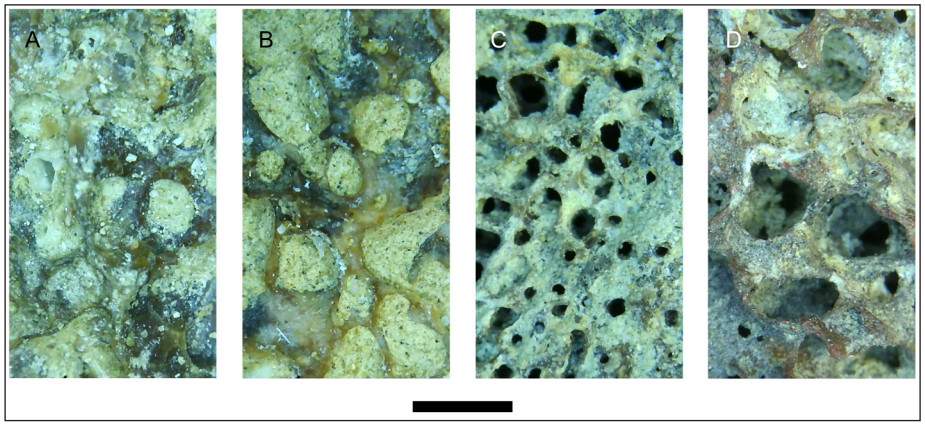

Fig. 7 - Internal bony structures of MGPT-PU 13864. Internal bone structure as exposed in the proximal portion of a rib (*m* in Fig. 13) showing lacunae and bony trabeculae. A, B) The lacunae are invaded by the sand of the Sabbie d'Asti Formation; the bony trabeculae are often lost. C) Small lacunae and bony trabeculae partially invaded by sand. D) Wide lacunae and bony trabeculae mostly free from sand. Scale bar equals 1 mm.

the whale carcass was deposited in a deep sea floor but this is not the case because the Sabbie d'Asti Formation represents an environment whose depth was about 30 m (Bisconti et al. 2021 and literature therein).

The bones are intensely fractured; the fractures mainly occur perpendicularly to the long axis of the long bones suggesting that the weight of the sediments after burial was the principal reason of the fractures. The weight of the sediment was probably responsible of some post-mortem deformation observed in the neural canals of many vertebrae which appear transversely slightly flattened. No shark teeth were found around or over the bones. The hypothesis of a burial occurring after a moderate time interval after the deposition on the sea floor is consistent with the general biostratinomic model provided by Bisconti et al. (2021a) for the Pliocene mysticetes from the Sabbie d'Asti Formation and this, together with observations on the articulation and good preservation of other Pliocene odontocetes from Piedmont (Bisconti et al. 2023a), supports the general validity of such a model.

Systematic palaeontology

Class **MAMMALIA** Linnaeus, 1758
Order **Cetacea** Brisson, 1762
Clade **Neoceti** Fordyce & Muizon, 2001
Parvorder **Odontoceti** Flower, 1867
Superfamily Physeteroidea Gray, 1868
Family Physeteridae Gray, 1821

Genus *Eophyseter* gen. nov.

Type species: *Eophyseter damarcoi* sp. nov., only included species.

Etymology: *Eo* is a Greek word (ἠώς) that means dawn, meaning ancestral, old. *Physeter* derives from the Greek φυσώ meaning blower.

Diagnosis of genus: *Eophyseter damarcoi* gen. nov. sp. nov. shows a unique morphology of the atlas, in the axis-bearing cervical block, in the proportions of the vertebral column and in the ulna. Diagnostic characters are the following: (1) the atlas is characterized by articular facets for the occipital condyles that protrude dorsally to the body of the vertebra and reach the height of the superior surface of the neural arch; (2) the articular surface for occipital condyles are comparatively wider than those of all the other physeteroids in which the atlas is preserved, and their ventromedial portion is comparatively longer; (3) in the axis-bearing cervical block, the epiphysis of the 7th cervical vertebra is dorsoventrally compressed and transversely widened to form showing an elliptical outline (it is transversely narrow and rounder in all the other physeteroids in which the axis-bearing block is preserved); (4) the lengths of the vertebral centra are comparatively more elongated than those of physeterids in which the vertebral column is known; in particular, in a long portion of the thoracic and lumbar regions of the vertebral column, the lengths of the centra are almost equal to the corresponding widths and heights (this pattern contrasts with that of extant sperm whales in which the length values are lower than those of heights and widths); (5) the posterior border of the ulna is posteriorly convex rather than being straight or concave as in other physeterids in which the ulna is preserved.

Eophyseter damarcoi gen. nov. sp. nov.

Figs 10-25

Holotype: MGPT-PU 13864, a partial skeleton including most of the vertebral column (a total of 36 vertebrae including seven cervicals subdivided into two blocks: one including the atlas, C_1, and the other including axis, C_2, and C_3-C_7 vertebrae), eleven thoracics, six lumbars and twelve caudals; the skeleton includes also the left scapula and left humerus, partial radius and ulna, part of the sternum, 15 ribs and one chevron. The holotype skeleton is currently on display in a temporary exhibition at MGPTA; for exhibition reasons, reconstructions of skull, mandibular rami and the left manus were added to the skeleton (Fig. 2).

Etymology: The patronymic *damarcoi* is to honor Piero Damarco (Fig. 2B) who coordinated and executed extensive preparation of the specimen and who dedicated his life to the discovery and curation of the fossil treasures of Piedmont, Northwest Italy.

Diagnosis: As for genus.

Type locality and stratigraphy: Parona (1930) stated that the specimen was found in the territory of the Valmontasca village, more precisely in "Regione Cavallino", in the municipality of Vigliano d'Asti (about 4 km South of Asti and about 45 km South-East of Torino, Piedmont, North-West Italy; Fig. 1). Nosenzo (2022) was able to find a living witness of the excavation made by Parona and Richard in 1929 and, together with him, could find the exact discovery site where the Sabbie d'Asti Formation extensively outcrops. The Sabbie d'Asti Formation was reviewed by Bisconti et al. (2021c; see also the literature cited therein for a full characterization of the Sabbie d'Asti Formation). Based on the evidence provided by Bisconti et al. (2021c and literature therein), the age of the Sabbie d'Asti Formation can be constrained between 3.2 and 3.0 Ma in the early Piacenzian; overall depth was limited to the upper 30 m; climate was mainly tropical-to-subtropical based on mollusk community analyses (Damarco 2009).

Description

Body size inference

Application of the equations (1)-to-(4) to MGPT-PU 13864 resulted in the following estimates. Equation (1) provides a total skull length of 5.19 m, equation (3) provides a result of 5.69 m. We thus estimate that the mean length of the skull of MGPT-PU 13864 based on these results is 5.44 m. Equation (2) results in a total skeletal length of 13.18 m and equation (4) provides an estimation of the total skeletal length of 12.47 m. Based on these estimations, we find that the mean skeletal length of MGPT-PU 13864 is 12.83 m. After correction, we estimate that the total body length of the intact animal is 15.1 m which is consistent with an adult age based on the life tables of the extant sperm whale (Omura et al. 1962; Nishiwaki et al. 1956).

In our knowledge, there are no life tables of the extant sperm whale in which the degree of fusion of the vertebral epiphyses to the vertebral bodies, or the degree of fusion of the limb epiphyses are put into relationships with the age of the individuals. Based on that, we can only make a rough estimation of the age of the specimen under investigation that derives from the observation of the complete fusion of the humeral epiphyses to the shaft of the humerus and on the large size of the individual. Based on these observations, we estimate that the individual was fully adult at the moment of its death.

Osteology

The skeleton includes most of the vertebral column together with ribs and two chevrons (Figs 8-16) and part of the forelimb (Figs 17-20). Vertebral measurements are provided in Table 3, ribs measurements are reported in Table 4 and forelimb measurements are presented in Table 5. Based on our counts and on comparisons with the extant sperm whale, we propose the following vertebral formula for *Eophyseter damarcoi*: 7C, 12T, 6+L, 12+Ca = 36. We estimate that about 10 caudal vertebrae and a couple of lumbars are missing because of biostratinomic processes able to remove them and move them apart. Therefore, the total estimated vertebral count of *E. damarcoi* including preserved and missing vertebrae and is 37+12 = 49. According to Flower (1868) and Omura et al. (1962) the

Vertebra[1]	CL	CW	CH	NCH	NCW
C_1	135	635	340	200	215
C_2-C_7	120	307	394	144	191
T_1	104	214	191	140	160
T_2	107	210	174	135	160
T_3	102	240	180	135	157
T_4	150	182	177	140	147
T_5	143	182	185	115	137
T_6	125	220	206	132	114
T_7	137	207	179	112	107
T_8	158	212	184	129	77
T_9	182	204	185	115	73
T_{10}	170	204	218	143.7	70.5
T_{11}	200	205	195	91	68
L_1	225	217	214	-	66.2
L_2	160	181	210	129	65
L_3	237	219	228	77	60.96
L_4	218	210	216	94	58.3
L_5	239	230	227	70.3	57
L_6	247	224	209	-	50.7
Ca_1	197	210	173	135	48.07
Ca_2	233	200	200	56	43.9
Ca_3	247	230	215	40	37
Ca_4	319	205	207	-	33
Ca_5	226	237	217	-	28
Ca_6	230	215	205	35.6	26.2
Ca_7	194	174	195	-	18.7
Ca_8	179	160	170	21	14
Ca_9	147	150	162	13	11
Ca_{10}	113	162	140	Neural arch absent	
Ca_{11}	74	147	109		
Ca_{12}	64	130	90		

Tab. 3 - Vertebral measurements (in mm) of the MGPT-PU 13864, holotype of *Eophyseter damarcoi* gen. nov. sp. nov.
[1]Caption: CH, centrum height; CL, centrum length; CW, centrum width; NCH, height of neural canal; NCW, width of neural canal.

Rib	Maximum chord[1]		Maximum transverse diameter[1]	
	Right side	Left side	Right side	Left side
1	630	705	143	140
2	980	880	90	90
3	430	835	92	75
4	800	940	70	65
5	605	930	40	75
6	781	788	60	68
7	572	690		60
8		652		63

Tab. 4 - Measurements of the ribs of MGPT-PU 13864, holotype of *Eophyseter damarcoi* gen. nov. sp. nov. in mm. [1]As preserved.

Character	mm
Scapula:	
anteroposterior diameter taken at proximal border	178
anteroposterior diameter from *margo caudalis to* apex of acromion	248
maximum proximodistal diameter	612
linear length of *margo caudalis*	500
linear length of *margo cranialis*	685
length of acromion	248
height of distal border of acromion	94
length of coracoid process	74
height of distal border of coracoid process	39
height of base of coracoid process	77
anteroposterior diameter of acetabular fossa	120
transverse diameter of acetabular fossa	137
Humerus:	
maximum proximodistal length	304
maximum anteroposterior diameter at proximal epiphysis including deltopectoral crest	178
length of deltopectoral crest	130
maximum length of shaft from ventral border of articular head	204
maximum anteroposterior diameter of articular head	130
maximum proximodistal diameter of articular head	125
anteroposterior diameter of distal epiphysis	175
transverse diameter of distal epiphysis	65
anteroposterior length of radial facet	90
anteroposterior length of ulnar facet	74
Radius:	
proximodistal length (as preserved)	254
anteroposterior diameter of shaft	90
distance from proximal epiphysis to radial process	60
anteroposterior diameter of proximal epiphysis	120
transverse diameter of proximal epiphysis	75
anteroposterior diameter of distal epiphysis	109
transverse diameter of distal epiphysis	95
maximum height x maximum width of ulnar facet	36x60
Ulna:	
Proximodistal diameter	232
Anteroposterior diameter distal to radial facet	75
Anteroposterior diameter of proximal epiphysis (as preserved)	60
Transverse diameter of proximal epiphysis	55
Anteroposterior diameter of distal epiphysis	135
Transverse diameter of distal epiphysis	42
Maximum height x maximum width of radial facet	41x29

Tab. 5 - Measurements in mm of the forelimb of MGPT-PU 13864, holotype of *Eophyseter damarcoi* gen. nov. sp. nov.

extant *Physeter macrocephalus* shows the following vertebral formula: 7C, 10-12T, 8L, 23-24Ca = 49-50.

Vertebral column. The cervical vertebrae include the atlas (C_1) and a block of fused vertebrae including the axis (C_2) and the other five vertebrae (C_3-C_7) (Fig. 8A-G). The atlas resembles that of the extant sperm whale very closely. According to the descriptions provided by Flower (1868) and Omura et al. (1962), the Vigliano sperm whale shows a trapezium-like overall outline of C_1 in which the dorsal and ventral surfaces are scarcely convex and the lateral sides are squared. In both the extant and the Vigliano sperm whales the articular facets for the occipital condyles are obliquely oriented with respect to the dorsoventral axis of the vertebra and mainly project dorsally and laterally. Their transverse diameter increases approaching the dorsal border therefore their shapes is almost triangular. The articular surfaces are scarcely concave and are ventrally separated by an intercondyloid incisure that is 34 mm in width; dorsally, they are separated by the dorsal border of the neural canal that is 215 mm in width.

The neural canal is between the articular facets for the articulation with the occipital condyles; it is broadly triangular and its lateral borders are externally convex. At about 180 mm from the dorsal border, the neural canal abruptly diminishes its transverse diameter and gets an elliptical shape; this ventral-most portion is interposed between the ventromedial borders of the articular facets for the occipital condyles and slightly dorsal to the intercondyloid incisure.

The neurapophysis is absent; the neural arc is reduced to a rod-like, straight bar running between the dorsomedial corners of the articular facets for the articulation with the occipital condyles.

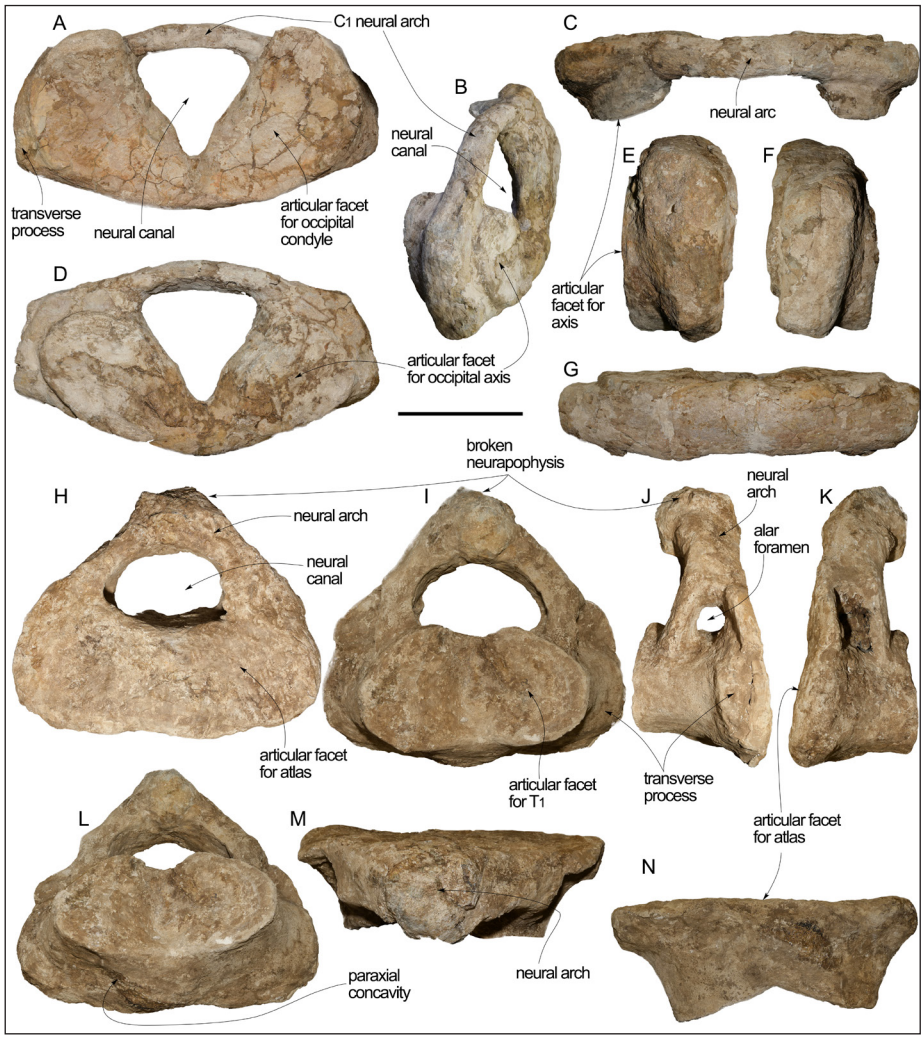

Fig. 8 - Cervical vertebrae of MGPT-PU 13864, holotype of *Eophyseter damarcoi* gen. nov. sp. nov. Atlas in A) anterior view; B) right dorsolateral view; C) dorsal view; D) posterior view; E) right lateral; F) left lateral; G) ventral views. Axis in H) anterior; I) posterior; J) right lateral; K) left lateral; L) posteroventral; M) dorsal; N) ventral views. Scale bar equals 10 cm.

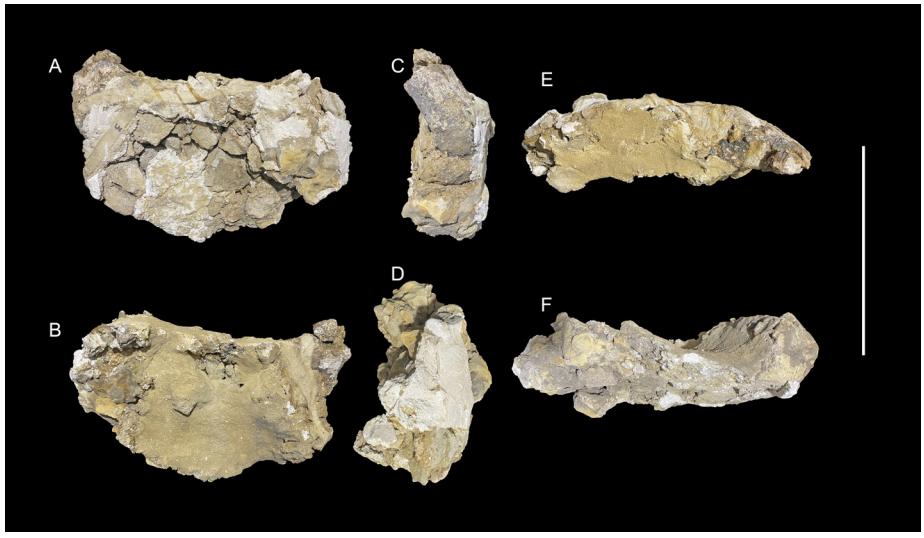

Fig. 9 - First thoracic vertebra in A) anterior; B) posterior; C) left lateral; D) right lateral; E) dorsal; and F) ventral views. Scale bar equals 20 cm.

The transverse processes are short and squared. The ventral border of the transverse processes is scarcely inclined dorsolaterally and forms a right angle with the lateral border which projects dorsally and medially. At the height of the dorsal surface of the neural arch, the lateral border of the transverse processes form a right angle and project medially to join the dorsal surface of the atlas.

There are no transverse foramina in the atlas of the Vigliano sperm whale.

Posteriorly, the articular facets for the axis are triangular and obliquely oriented with respect to the

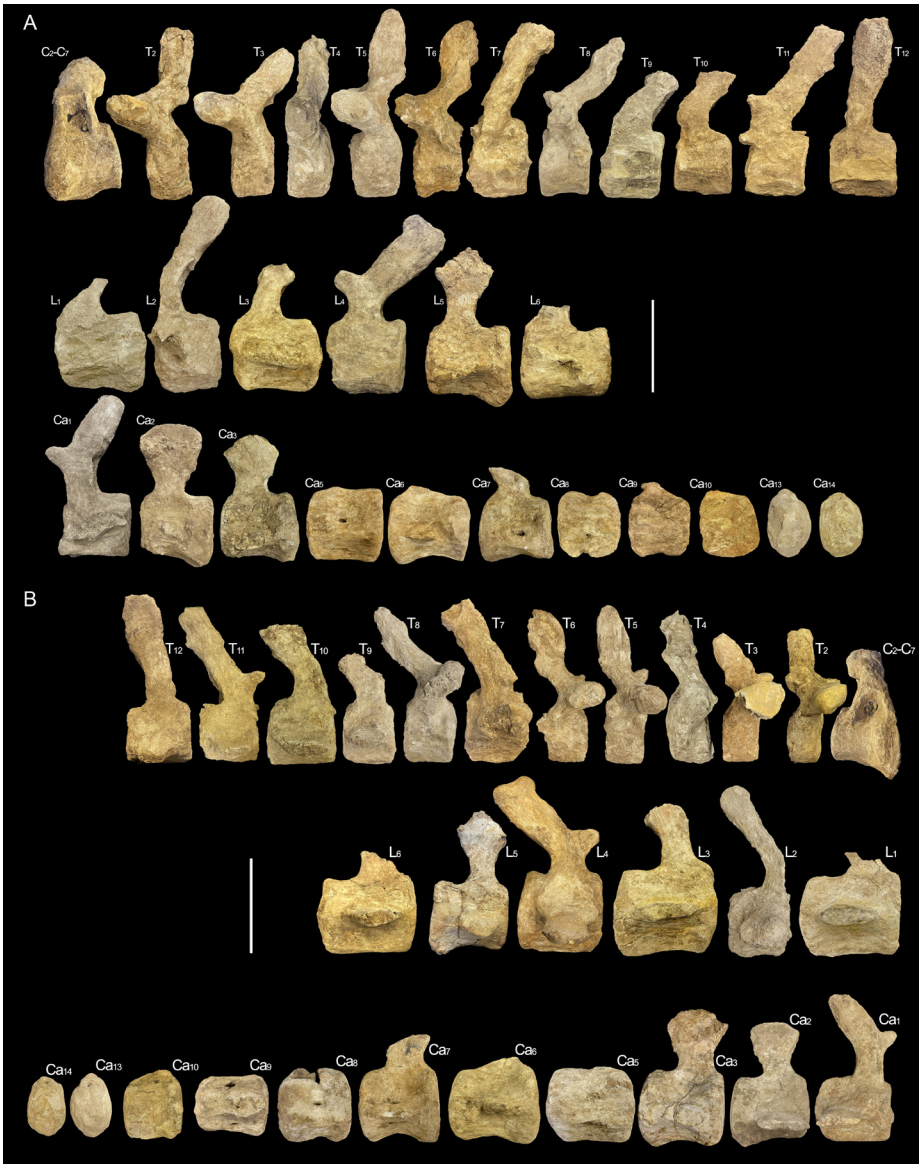

Fig. 10 - Vertebral column of MGPT-PU 13864, holotype of *Eophyseter damarcoi* gen. nov. sp. nov. A) Left lateral view. B) Right lateral view. Caption: C) Cervical vertebrae; T, thoracic vertebrae; L, lumbar vertebrae; Ca, caudal vertebrae. Scale bar equals 20 cm.

dorsoventral axis of the vertebra. The articular facets protrude for *c.* 10 mm from the body of the vertebra. A wide incisure (75 mm in width) separates ventromedial apices of the articular facets.

The ventral surface of the atlas body is anteroposteriorly thicker along the median axis of the vertebra where it is also more ventrally convex and rounded.

The block including the vertebrae C_2-C_7 is badly preserved (Fig. 8H-N); its maximum transverse diameter, including the transverse processes of the axis, is 470 mm and its maximum height, including the neural arch, is 394 mm. In anterior view, this block shows the anterior surface of the axis (C_2). The odontoid process is low and wide and its surface shows signs of abrasion. The neural arch is low, triangular and does not show a well-developed neural apophysis; rather, its dorsal surface is widely rounded and scarcely protruding. The superior portion of the neural arch is thick (111 mm in height from the roof of the neural canal to the apex of the neural arch) and bears a transverse foramen characterized by an oval outline. The neural canal is transversely expanded and shows a rectangular outline.

In posterior view, the block shows the posterior aspect of the seventh cervical vertebra. The articular facet for the articulation with the first thoracic vertebra is badly eroded and flattened. It is subdivided into two parts by an incision developed from the dorsal border of the facet at the middle of the width of the vertebra. The right and left portions are respectively *c.* 174 and *c.* 150 mm in height and a shallow fossa is interposed between them. The neural canal is low, wide and elliptical.

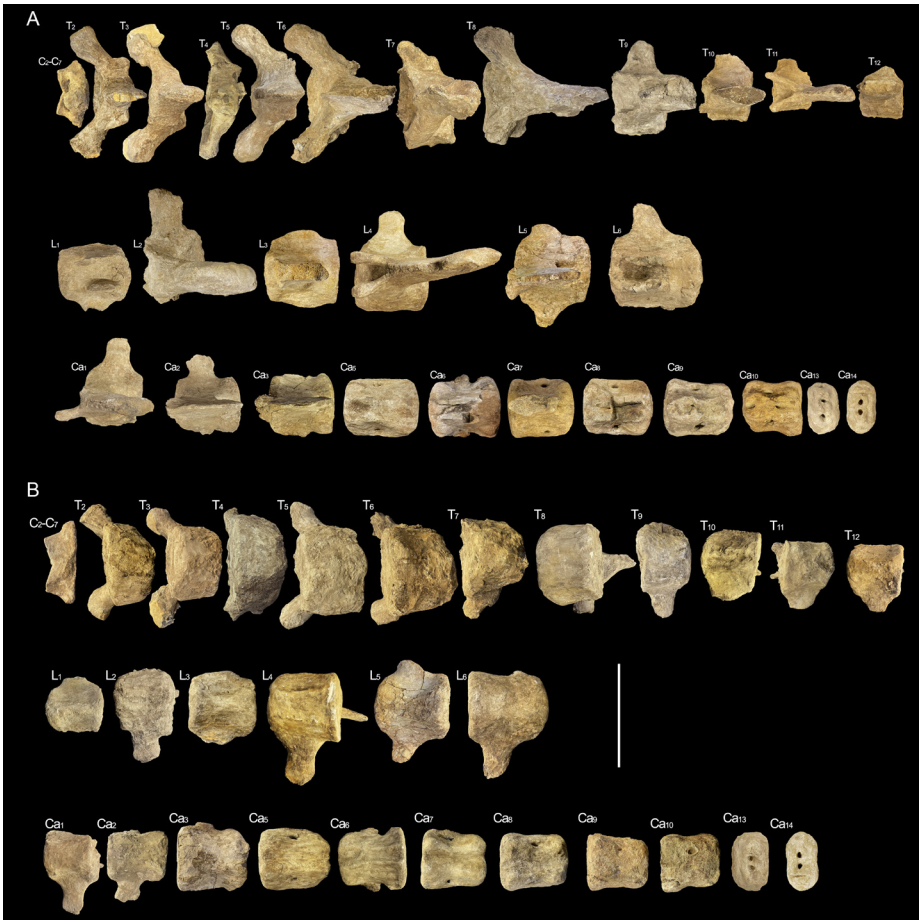

Fig. 11 - Vertebral column of MGPT-PU 13864, holotype of *Eophyseter damarcoi* gen. nov. sp. nov. A) Dorsal view. B) Ventral view. Caption: C) cervical vertebrae; T, thoracic vertebrae; L, lumbar vertebrae; Ca, caudal vertebrae. Scale bar equals 20 cm.

The neural arch of the whole block is formed by a single neural apophysis due to the fusion of the apophyses of the cervical vertebrae C_2-C_7. The lateral wall of the neural canal is formed by an anteriorly-placed lateral wall belonging to the axis (C_2) that is slender and a posteriorly-placed lateral wall of pillar-like shape that belong to the other cervical vertebrae (C_3-C_7). These two lateral walls of the neural canal bound a transversely-developed alar foramen that connects the neural canal with the outside of the block. Transverse processes are absent in the vertebrae C_3-C_7 and only a short and squared transverse process is observed for the axis.

Completeness of the vertebral column is shown in Table 2 and Supplementary Information Fig. S1, and vertebral measurements are provided in Table 3. Apart from the first thoracic vertebra (T_1) that is largely broken and reassembled in an almost not intelligible way (Fig. 9), the other eleven preserved thoracic vertebrae show variable outlines of the anterior and posterior epiphyses of the centra. (Figs 10-13). The first thoracic vertebra shows a dorsoventrally compressed centrum and robust lateral portions of the neural arch. The outline of the epiphysis of T_2 is similar to a half-circle with a straight dorsal border; the outlines of the epiphyses of T_3-T_6 are grossly hexagonal; the outline of the anterior epiphysis with the T_6 is roughly octagonal and those of T_8-T_{12} are hexagonal with sharper corners. The tubercle-like transverse processes of T_2-T_8 are connected to the lateral walls of the neural canals; the flat transverse processes of the subsequent thoracic vertebrae are connected to the lateral surfaces of the vertebral centra.

In lumbar vertebrae, a ventral keel is observed in L_1-L_4 and also in one of two of the last thoracics (T_{11} and T_{12}) and the transverse processes are elongated and flat.

Metapophyses are located dorsal to the neural arch along most of the vertebral column; separate metapophyses are present in T_2-T_{11}, L_2 and L_4. Metapophyses are fused in a single structure in L_3, L_5, L_6, and Ca_1-Ca_3 and Ca_7. In T_{12} the metapophysis is poorly preserved; in the other vertebrae not mentioned above the metapophyses are not preserved.

In anterior view, the neural canal is elliptical and very wide in T_2-T_8; it is triangular and higher than wide in T_9-Ca_3 and Ca_5-Ca_6. In Ca_7-Ca_8, the neural ca-

Fig. 12 - Vertebral column of MGPT-PU 13864, holotype of *Eophyseter damarcoi* gen. nov. sp. nov. in anterior view. Caption: C, cervical vertebrae; T, thoracic vertebrae; L, lumbar vertebrae; Ca, caudal vertebrae. Scale bar equals 20 cm.

nal is small-sized and indistinct in shape; in the last caudal vertebrae from Ca_8, the neural canal is closed.

The superior portion of the neural arch disappears in Ca_{13}-Ca_{14}. In these vertebrae, the foramen in the transverse process is close to the neural arch; the two foramina are present in a ventral fossa. In Ca_{13} the foramina in the transverse processes are located within a dorsomedian fossa whereas the couple of foramina located in the ventromedian fossa are placed more distantly. In Ca_{14} there is a transverse fissure instead of a dorsomedian fossa; in this fissure two foramina are located that correspond to the

Fig. 13 - Vertebral column of MGPT-PU 13864, holotype of *Eophyseter damarcoi* gen. nov. sp. nov. in posterior view. Caption: C, cervical vertebrae; T, thoracic vertebrae; L, lumbar vertebrae; Ca, caudal vertebrae. Scale bar equals 20 cm.

foramina for the transverse processes; in the ventromedian fossa, the foramina are more closely spaced.

*Chevrons***.** Two chevron bones and a partial third one are well-preserved (Fig. 14). The larger chevron (Fig. 14A-D) includes a ventral process that is anteroposteriorly and dorsoventrally elongated (maximum dorsoventral diameter, 101 mm; maximum dorsoventral diameter, 173 mm); its lateral surface is flat and straight. The anteroposterior length of the ventral process is 104 mm and its height from the peduncles bearing the attachment sites for the caudal vertebra is 100 mm. The ventral border of the ventral process is straight and its anterior and posterior corners are rounded. The attachment sites for the caudal vertebra are divergent from the dorsoventral axis and their distance increases towards the dorsal border of the bone. The articular facets for the caudal vertebra are transversely flat (maximum transverse diameter is 35 mm in the left and 39 mm on the right) and anteroposteriorly convex. The fossa included between the peduncles of the articular facets for the caudal vertebra, is elliptical in anterior view and 23 mm deep. The distance between the articular facets for the caudal vertebra is 31 mm. Judging from the illustrations provided by Omura et al. (1962), we suggest that this chevron is the number 7 (count starting from the anterior one).

A second chevron (Fig. 14E-I) is anteroventrally shortened with respect the previous one; the

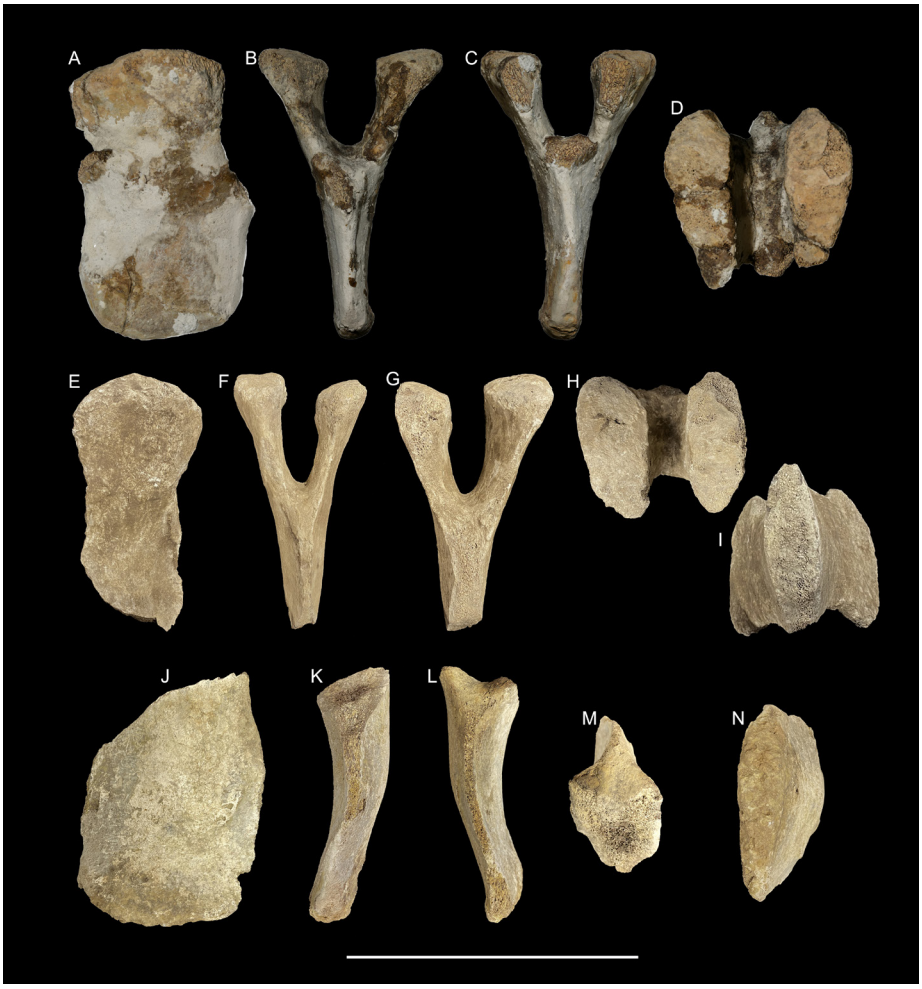

Fig. 14 - Chevrons of MGPT-PU 13864, holotype of *Eophyseter damarcoi* gen. nov. sp. nov. First chevron (No. 7). A) Right lateral view. B) Anterior view. C) Posterior view. D) Dorsal view. Second chevron (No. 2). E) Right lateral view. F) Anterior view. G) Posterior view. H) Dorsal view. I) Ventral view. Third chevron (No. 6). J) Right lateral view. K) Anterior view. L) Posterior view. M) Dorsal view. N) Ventral view. Scale bar equals 20 cm.

fossa between the articular processes is elliptical in anterior and posterior views; the articular processes are clavate in anterior view and show dorsally convex articular surfaces. The ventral, crest-like portion bears a keel that protrudes ventrally for about 115 mm. The maximum transverse diameter of the fossa located between the articular processes is about 20 mm and the maximum height of the ventral portion is about 100 mm. Size and shape suggest that this chevron was the second of the series starting from the anterior-most position according to Omura et al. (1962) figures.

The third chevron (Fig. 14J-N) is only represented by the ventral portion as the articular processes are broken. This particular chevron was published by Richard (1930) who used its peculiar morphological characteristics to establish a relationship between the Vigliano sperm whale and the extant southern sperm whale population that was known as *Physeter australis* at the times of Richard's publication. This chevron is visibly asymmetrical in that the dorsoventral axis of the ventral portion is not vertical in anterior and posterior views. Rather, the main axis of this portion is obliquely directed to the left side. The ventral portion of this chevron is anteroposteriorly elongated in lateral view; this observation suggests that it was located close to the first chevron described above in the living animal. The main anteroposterior diameter of the ventral portion is about 110 mm and this suggests that this chevron was probably the sixth in the series based on the proportions published by Omura et al. (1962). The maximum height of this chevron is about 160 mm.

Ribs. It is possible to count seven ribs from the right side and eight ribs from the left side (Fig. 15). Maximum chords and maximum anteroposterior diameters of the shafts are provided in Table 4. The first rib is preserved on both sides (ribs *a* and *h* in Fig. 15). It include a complex head (see below), a curved shaft and a transversely expanded epiphysis. The head of the first rib shows a rounded capitulum that is morphologically similar to that described by Flower (1868) in a skeleton of a southern sperm

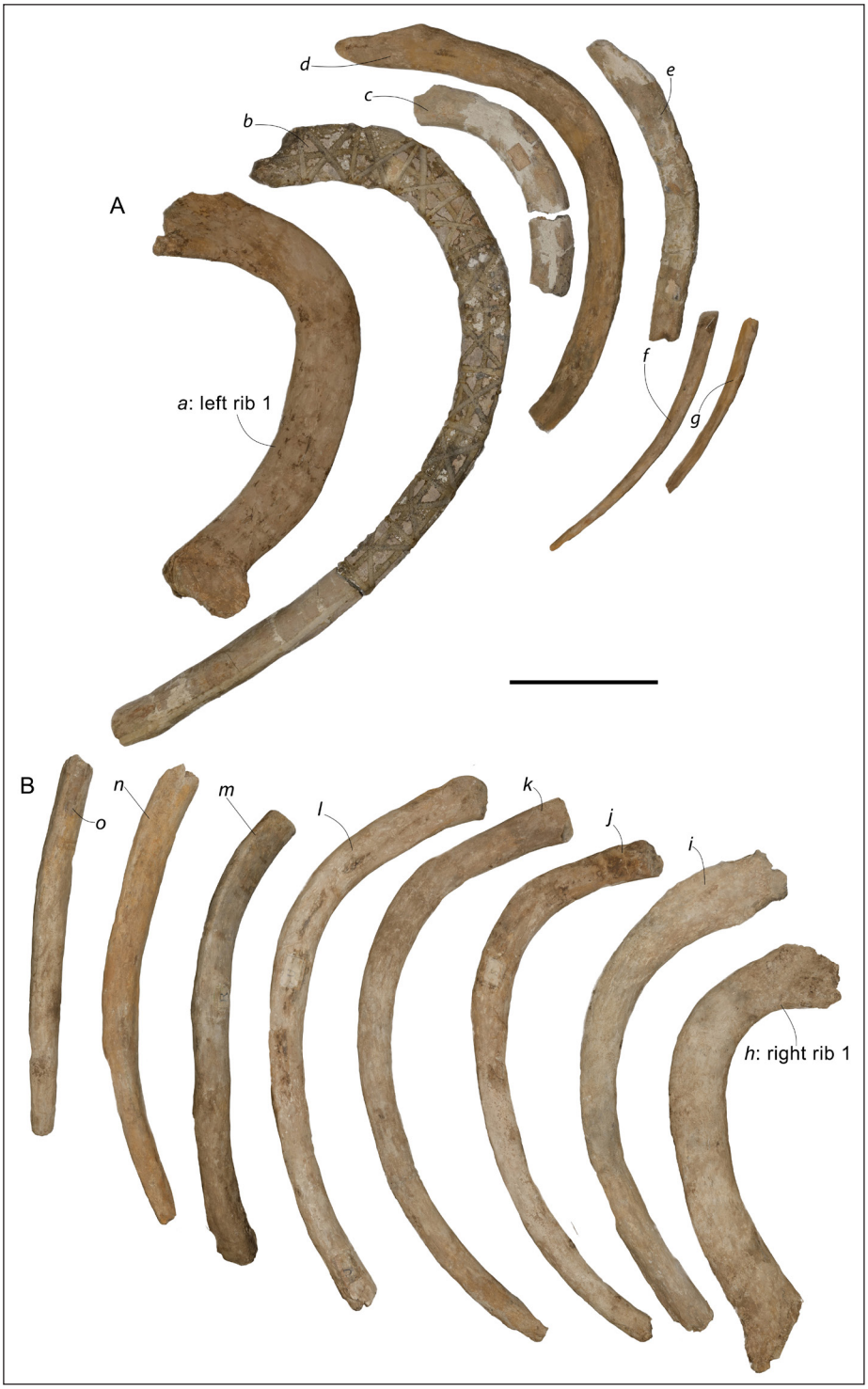

Fig. 15 - Ribs of MGPT-PU 13864, holotype of *Eophyseter damarcoi* gen. nov. sp. nov. A) Ribs from the right side (*a*, *b*, *c*, *d*, *e*, *f* and *g*). B) Ribs from the left side (*h*, *i*, *j*, *k*, *l*, *m*, *n* and *o*). Scale bar equals 20 cm.

whale. Differing from the latter, in the northern sperm whale described by Omura et al. (1962) the capitulum of the first rib is straighter. The tuberculum of the first rib is triangular and slender (30 mm in basal diameter and 50 mm in length) and differs from both the tubercula described in the first rib by Flower (1868) and Omura et al. (1962) that are shorter and higher; it is separated from the capitulum by a wide and concave incisure. The distal expansion of the first rib is formed by two distinct protrusions on the opposite sides of the rib; these protrusions form a rough articular surface for the sternum. On the posterior surface of the first right rib, at the level of the distal epiphysis, a wide concavity is present but it is absent in the first left rib. The anterior surface of the shaft of the first rib is proximally flat and the shaft

Fig. 16 - Sternum of MGPT-PU 13864, holotype of *Eophyseter damarcoi* gen. nov. sp. nov. A-E) Different views of the right manubrium bone. F-J) Different views of the left manubrium bone. K) Ventral view of the body bone. L) Superior view of the left manubrium bone. M) Superior view of the right manubrium bone. N-Q) Different views of the left body bone. Note that E, J and K views are superimposed on the outline of the sternum of an extant sperm whale in inferior view redrawn with modification from Omura et al. (1962). Note also that L, M and Q views are superimposed on the outline of the sternum of an extant sperm whale in superior view redrawn with modification from Omura et al. (1962). Scale bar equals 20 cm.

is thin with respect to the distal epiphysis where it is visibly thicker.

A possible second rib is present on the right side (rib *b* in Fig. 15). It includes a strongly arched shaft with bifid head including an elongated and squared tuberculum (60 mm in basal diameter and 120 mm in length). The other ribs from the right side are fragmentary; they include segments of ribs posterior to the second and only two of them still include the articular heads. In one case (rib *d* in Fig. 15), the single head includes an elongated and triangular tuberculum (225 mm in length) and a sharp corner probably corresponding to the iliocostal tuberosity which is located at a distance of 185 mm from the tubercular apex. In the second case (rib *e* in Fig. 15), the single head shows the basis of an elongated tuberculum missing the apex.

On the left side the ribs are more complete but mostly posterior ribs are present. A possible second rib is badly damaged (rib *i* in Fig. 15). The subsequent ribs show truncated proximal and distal epiphyses. The internal angle of these ribs diminishes approaching the posterior portion of the ribcage. The inferred last two left ribs (ribs *n* and *o* in Fig. 15) are substantially straight.

Iliocostal tuberosities are indistinct in most ribs with the exceptions of ribs *k*, *l* and *m* (Fig. 15) where the tuberosities are evident and well-developed. These ribs may correspond to ribs 4 and 5 as described by Omura et al. (1962).

*Sternum***.** Three fragments of the sternum are preserved (Fig. 16). The two bones forming the manubrium are juxtaposed along the longitudinal axis of the animal body and form a median opening showing a vaguely-olive outline. The right manubrium bone is more fragmentary and is represented by a central portion of the plate preserving part of

both the anteromedial and the anterolateral edges showing that the lateral border projects posteriorly toward the longitudinal axis of the bone (Fig. 16A-E). Its main transverse diameter is 430 mm, its main anteroposterior diameter is 340 mm and its thickness ranges from 15 to 52 mm.

The left manubrium bone is represented by an anterior portion that shows an almost rectangular shape (Fig. 16F-K). Its anterior border is slightly concave; the lateral corner is approximately squared and the lateral edge projects posteriorly converging toward the longitudinal axis of the bone. The main transverse diameter of this portion is 585 mm, its main anteroposterior diameter is 328 and its thickness ranges from 106 to 125 mm.

On the left side, a portion of the body of the sternum is preserved that shows a convex median border, an overall triangular outline and a concave lateral edge (Fig. 16K, N-P). The main transverse and anteroposterior diameters are, respectively, 381 and 282 mm and its thickness ranges from 20 to 65 mm.

All these fragments are flat. Most of the sternum portions are still unprepared and the original tape and plaster used by Camillo Richard during the excavation are still in place (Fig. 16E, M, K, Q).

*Scapula***.** A largely complete left scapula is present (Figs. 17, 18) that shows a long proximodistal diameter and a short anteroposterior diameter (Table 5). Even though the dorsal border is not complete, based on what is preserved it can be inferred that it is straight in outline. The anterodorsal corner is wide and rounded. The rostral margin is sinuous. The posterodorsal corner of the scapula is triangular with obtuse apex. The caudal margin is uniformly concave.

In lateral view, the scapular spine is low and shows a triangular cross-section; it diminishes its height towards the proximal border and disappears at about 80 mm from it. The supraspinous fossa is anteroposteriorly short; it widens anteroposteriorly towards the proximal border. Posteriorly, the fossa for the teres muscle is well-bordered by a rounded bony strip that obliquely runs from the proximal border to the caudal margin. The subspinous fossa is wide and concave.

The acromion is a large process projecting anteriorly from the base of the scapular spine. It shows a broadly rectangular shape and its anterior

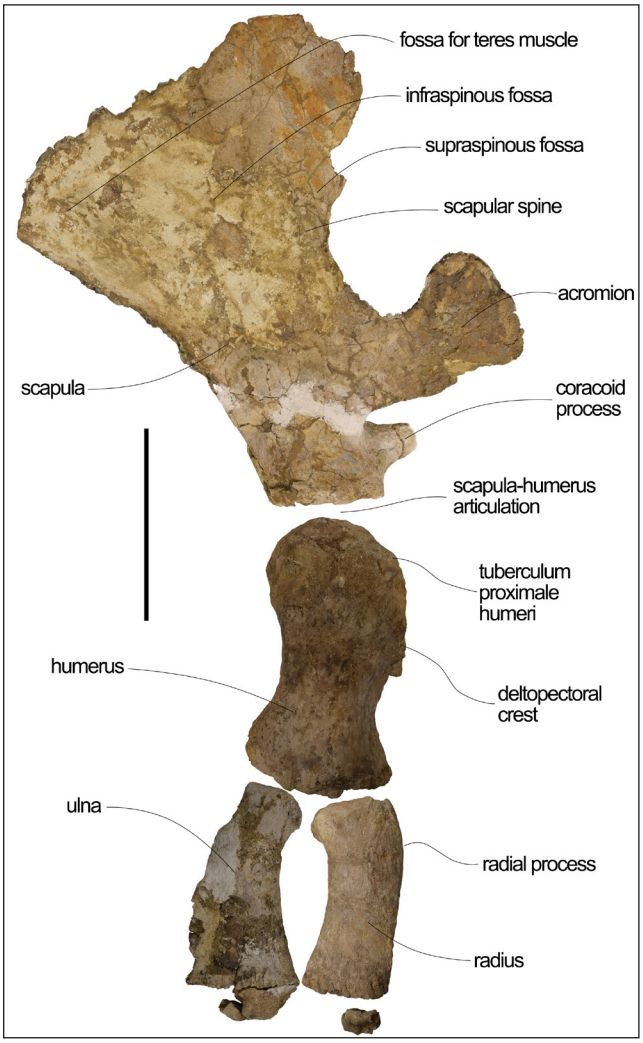

Fig. 17 - The forelimb of MGPT-PU 13864, holotype of *Eophyseter damarcoi* gen. nov. sp. nov. Scale bar equals 30 cm. The scapula is mirrored.

border protrudes as far as the anterodorsal corner does. The anterior border of the acromion shows rounded corners. The superior border of the acromion is remarkably concave whereas the inferior border is straight. The coracoid process is shorter than the acromion; it is placed immediately superior to the glenoid fossa of the scapula and projects anteriorly and distally to reach a length that is about one-third of the length of the acromion. The shape of the coracoid process is approximately triangular with anteriorly converging superior and inferior borders; the apex is squared-off. The overall aspect of the coracoid process is that of a stocky, robust and short structure.

In medial view, the surface of the scapula is largely reconstructed because it suffered heavy damage after burial. As a whole, the subscapular fossa appears flat and wide lacking anatomical structures

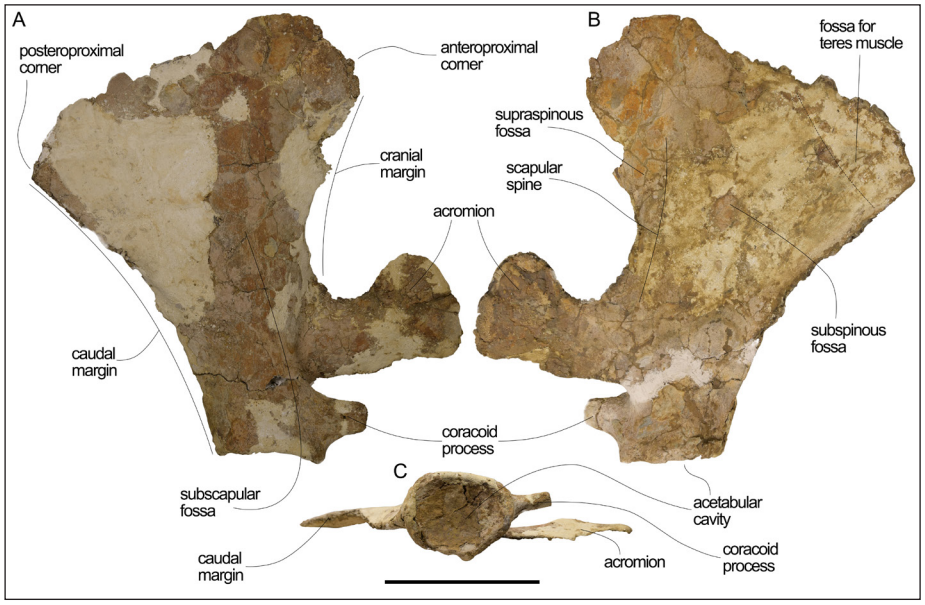

Fig. 18 - Left scapula of MGPT-PU 13864, holotype of *Eophyseter damarcoi* gen. nov. sp. nov. A) Medial view. B) Lateral view. C) Ventral view showing the glenoid cavity for articulation with humerus. Scale bar equals 20 cm.

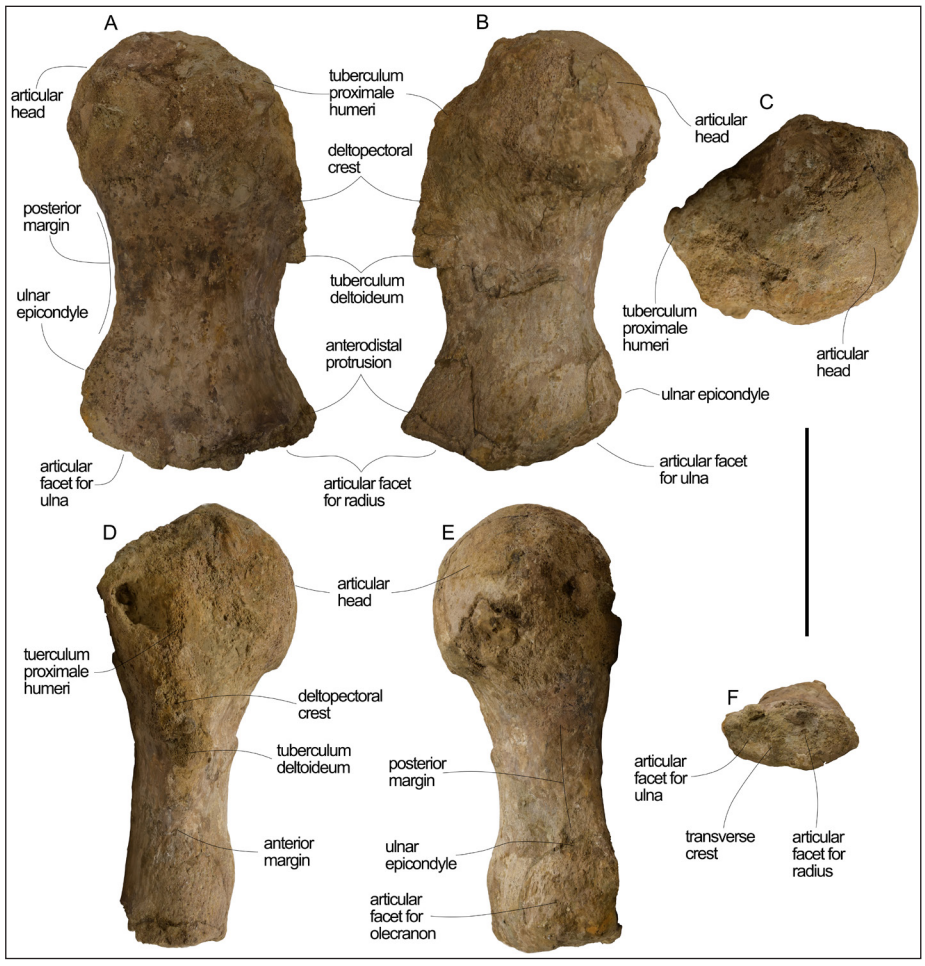

Fig. 19 - Left humerus of MGPT-PU 13864, holotype of *Eophyseter damarcoi* gen. nov. sp. nov. A) Lateral view. B) Medial view. C) Proximal view. D) Anterior view. E) Posterior view. F) Distal view. Scale bar equals 20 cm.

to be described. The medial aspect of the acromion shows that a shallow fossa is located on its superior border close to its base and that the medial surface of the acromion is convex.

The glenoid fossa is shallow and shows an elliptical outline.

Humerus. Overall, the left humerus is a robust structure (Figs. 17, 19). In the osteological description of the humerus, we will use the terminology provided by Benke (1987). The articular head of the humerus is uniformly rounded and shows a ventrally convex external border that can be observed in medial view.

Fig. 20 - Distal forelimb elements of MGPT-PU 13864, holotype of *Eophyseter damarcoi* gen. nov. sp. nov. Ulna in A) medial; B) lateral; C) posterior; D) anterior; E) distal; F) proximal views. Radius in G) lateral view; H) medial view; I) fragment of radial epiphysis; J) posterior view; K) anterior view; L) distal view; M) proximal view. Scale bar equals 20 cm.

The articular head protrudes posteriorly with respect to the posterior margin of the shaft that is straight. Distally, the ulnar epicondyle (corresponding to the facet for articulation for the olecranon process of the ulna) protrudes posteriorly forming an obtusely-triangular tubercle in lateral and medial views. In posterior view, the ulnar epicondyle resembles a short rectangle. The tuberculum deltoideum (corresponding to the anterodistal corner of the humerus) forms an anteriorly-projecting, triangular protrusion.

The tuberculum proximale humeri is low and obtuse; it is located anterior to the anterior margin of the articular head of the humerus. The deltopectoral crest is straight and long; it is robust and triangular in cross-section. The tuberculum medial humeri is triangular and is connected to the anterior margin of the shaft by a sharp angle. In cross section, the humeral shaft shows a convex medial surface and a mostly flat lateral surface. The distal epiphysis shows that both the articular facets for radius and ulna are characterized by long anteroposterior diameters and narrow transverse diameter. These facets are separated by a low transverse crest.

*Radius***.** The radius consists of a short and robust bone characterized by concave posterior border and convex anterior edge (Figs. 17, 20). The maximum convexity of the anterior border is located proximally, slightly below the proximal epiphysis and is thought to be homologous to the radial process of archaeocetes (Bisconti & Carnevale 2022). The lateral surface is flatter than the medial surface that is more externally convex. The proximal epiphysis is obliquely oriented with respect to the long axis of the radius and its anterior border is raised with respect to its posterior border. Slightly below the posterior border of the proximal epiphysis, an articular facet for the ulna is found that is approximately pentagonal and that is 60 mm in transverse width and 35 mm in proximodistal diameter. Both the proximal epiphysis and the distal end of the shaft are transversely compressed and show an anteroposteriorly elongated and transversely narrow outline. The whole radius is transversely compressed and shows a lozenge-shaped outline in cross-section (not shown).

A fragment of the distal epiphysis is detached from the radius and includes a small, irregular bony

element that fits the anterior portion of the distal surface of the bone.

*Ulna***.** The ulna is comparatively short and robust (Figs. 17, 20). Its posterior border is posteriorly convex and its anterior border is anteriorly concave. The anteroposterior diameter increases toward the distal portion where a long distal epiphysis is still attached to the shaft. The proximal epiphysis is small and rectangular in outline. A small and elliptical articular facet for the radius is located slightly below the anterior border of the proximal epiphysis. The olecranon is lost; the place where the olecranon was attached is located below the posterior edge of the proximal epiphysis and shows traces of breakage and roundish borders suggesting that the detachment of the olecranon occurred before the burial of the skeleton. Posterior and anterior edges of the ulna are sharp and crest-like and the ulna, like the radius, is transversely compressed with a more externally convex medial surface than the external surface that is almost flat.

Taken together, radius and ulna in articulation are joined proximally at the level of the articular faces located closely to their proximal epiphyses, and probably at the level of the anteroventral corner of the ulna and the posteroventral corner of the radius; an olive-shaped window is located between their respective shafts as in the extant sperm whale.

Morphological comparisons

Apart from the conspicuous differences in linear measurements of the post-cervical portions of the vertebral column that will be described elsewhere in this paper, here we focus on the morphologies of the atlas (C_1), the block including the axis and the other cervical vertebrae (C_2-C_7) and the forelimb.

Atlas

The atlas of *Physeter macrocephalus* is schematically illustrated in Fig. 21A, B in anterior view. In this species there is a certain degree of variation in this vertebra as the neural arch may be flat or arched, the neural spine may be absent or present, the ventral portion of the neural canal may be transversely narrow or wide, and the transverse processes are squared and protruding. In *Eophyseter damarcoi*, the atlas shows a mix of the above characteristics in that its neural arch is arched but lacks the neural spine, the ventral portion of the neural canal shows an intermediate proportional size with respect to *P. macrocephalus* (Fig. 21C). The transverse processes are short and rounded but this may be due, at least in part, to post-depositional erosion of the external surface of the atlas.

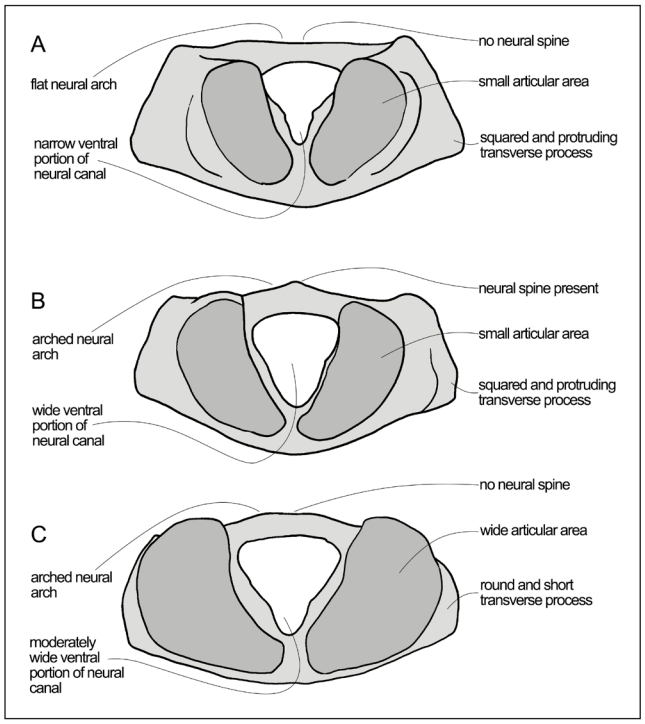

Fig. 21 - Comparative plate showing the first cervical vertebra (atlas) in anterior view in the extant sperm whale, *Physeter macrocephalus*, and MGPT-PU 13864, *Eophyseter damarcoi* gen. nov. sp. nov. A) Scheme of the atlas of *P. macrocephalus* from southern hemisphere modified from Flower (1864). B) Scheme of the atlas of *P. macrocephalus* from northern hemisphere modified from Omura et al. (1962). C) Scheme of the atlas of *E. damarcoi*. Not to scale. Characters discussed in the text are indicated.

Among stratigraphically older species, the physeteroid atlas IRSNB M. 524 previously assigned to *Eudelphis mortezelensis* (Du Bus, 1872), that is now considered an indeterminate physeteroid species (Lambert 2008), shows an atlas that is similar to that figured in Fig. 21B in that is shows an arched neural arch bearing a neural spine, squared and ventrally-protruding transverse processes but, differing from the more recent species, it shows a wide and broadly rounded neural canal and small articular surfaces for the occipital condyles (Abel 1905).

In *Zygophyseter varolai* Bianucci & Landini, 2006 the atlas is morphologically divergent from that of

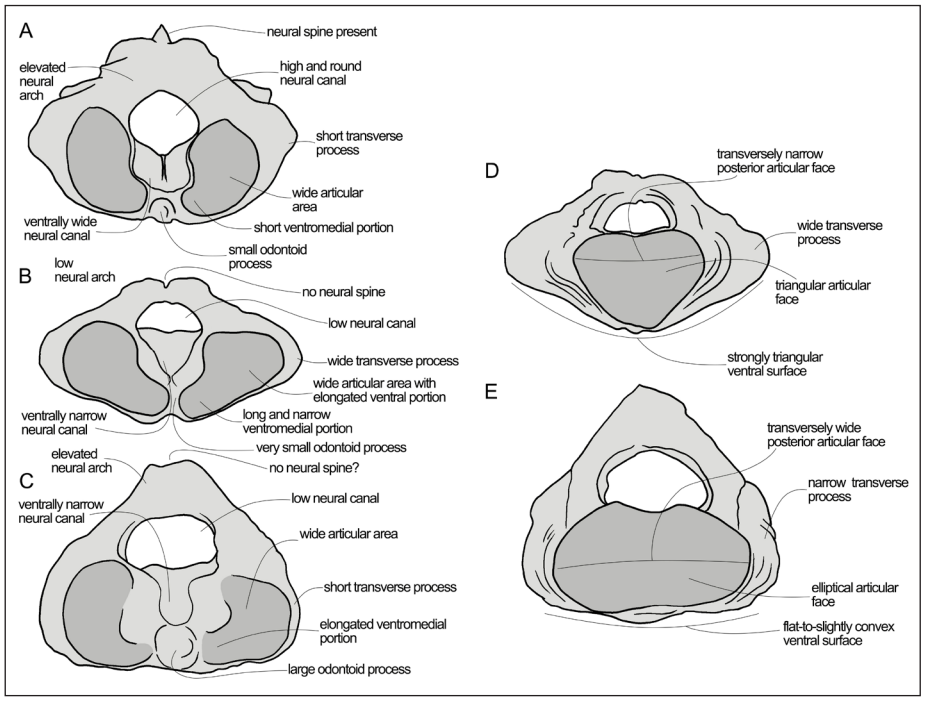

Fig. 22 - Comparative plate showing the block of cervical vertebrae including C_2-C_7 in the extant sperm whale, *Physeter macrocephalus*, and MGPT-PU 13864, *Eophyseter damarcoi* gen. nov. sp. nov. A) Scheme of the cervical block of *P. macrocephalus* from southern hemisphere in anterior view modified from Flower (1864). B) Scheme of the cervical block of *P. macrocephalus* from northern hemisphere in anterior view modified from Omura et al. (1962). C) Scheme of the cervical block of *E. damarcoi* in anterior view. D) Scheme of the cervical block of *P. macrocephalus* from northern hemisphere in posterior view modified from Omura et al. (1962). E) Scheme of the cervical block of *E. damarcoi* in posterior view. Not to scale. Characters discussed in the text are indicated.

IRSNM M. 524, *E. damarcoi* and *Physeter macrocephalus* in that the transverse process is rod-like; in this species the neural canal is wide and rounded with a broadly triangular ventral portion (Bianucci & Landini 2006). A similar morphology is exhibited by an indeterminate physeteriod from the Miocene of the Pietra Leccese Formation in southern Italy (Peri et al. 2020) and by *Cozzuoliphyseter rionegrensis* Paolucci et al., 2020. In these species the transverse process shows a rod-like morphology; in *C. rionegrensis*, the atlas is slightly more complete than in *Z. varolai* and the other Italian specimen and shows a wide and round neural canal together with an arched neural arch, and presence of a neural spine.

The partial atlas of *Placoziphius duboisi* Van Beneden, 1869 from the Miocene of Belgium shows a ventrally-protruding and roundish transverse process and an arched neural arch with a broad neural canal characterized by a wide ventral portion (Lambert 2008). In this species it is not possible to distinguish a ventromedial portion of the articular surfaces for the occipital condyles. The atlas of *Physeterula dubusi* Van Beneden, 1877 is scarcely preserved and shows only a wide ventral portion of the neural canal with wide articular facets for the occipital condyles (Lambert 2008).

In the living *Kogia breviceps* the atlas is transversely shortened with respect to that of *Physeter macrocephalus* and *E. damarcoi*; the neural process is present but the transverse processes are transversely reduced. In *Kogia* the cervical vertebrae are fused to each other with the exception of the last cervical vertebra that is fused to the others only by its neural arc while its centrum is free (Pinedo 1987; Omura et al. 1984)

Axis

The block including the cervical vertebrae C_2-C_7 shows remarkable individual variation in the extant *Physeter macrocephalus* (Fig. 22A, B). In an individual from the southern population of the living sperm whale represented by Flower (1864), in anterior view, the axis shows a high and round neural canal with a wide and elliptical ventral portion, presence of neural spine, roundish outline, small odontoid process and wide articular areas for C_1 in which the ventromedial portion is small (Fig. 22A). In an individual from an extant northern population (Omura et al. 1962), the outline of the block is wider, the neural canal is low and almost rectangular with a triangular ventral portion, the neural spine is absent and the wide articular areas for C_1 show an elongated and narrow ventromedial portion (Fig. 22B). In *Eophyseter damarcoi*, the neural canal is low and almost rectangular with a narrow and squared ventral portion, the neural spine is lost but the upper portion of the neural arch is eroded so that its presence cannot be ruled out, the articular surfaces for C_1 are wide with an elongated ventromedial portion, the odontoid process is large. In posterior view,

it was possible to only compare one individual from Omura et al. (1962) and *E. damarcoi* because the posterior view of the second cervical block is not represented in literature. The differences between this extant sperm whale individual and *E. damarcoi* are even more marked in posterior view (Fig. 22D, E) as it is clear that in the extant sperm whale, the ventral surface of the block is triangular but it is flat-to-slightly convex in *E. damarcoi*, the outline of the neural canal is squared in the extant species but rounded in *E. damarcoi*, the posterior face of the vertebral centrum is transversely narrow and heart-shaped in the extant species but it is elliptical and comparatively much wider in *E. damarcoi* and the transverse processes are much more protruding in the extant species but short in *E. damarcoi*.

In our knowledge there is only one description of the axis of a fossil sperm whale in the literature, that of *Cozzuoliphyseter rionegrensis* (Paolucci et al. 2020). In this species, the block including the axis and the other non-atlas cervical vertebrae shows that the neural canal is high and dorsally rounded; moreover, the transverse processes of the block are short and rounded and the posterior face of the centrum of C_7 is transversely short and vaguely heart-shaped. A large odontoid process and a high neural spine were figured in the indeterminate Miocene physeteriod from Antwerp, Belgium, by Peters & Monteiro (2005).

Forelimb

A comparative plate showing the skeletons of the forelimbs of different individuals of *Physeter macrocephalus* and *Eophyseter damarcoi* is presented in Fig. 23. As shown, the overall proportions of the forelimb are similar in these three examples but differences are observed in anatomical details. In the the extant sperm whale scapula (Fig. 23A), the cranial margin may be convex or straight (Fig. 23B) and visibly concave in *E. damarcoi* (Fig. 23C). The supraspinous fossa is differently extended in the extant sperm whales where it may show scarce extent or wide extent with *E. damarcoi* sharing the small extent. The shape of the acromion is variable in the extant sperm whale in that it may show a concave dorsal border of the acromion (like that of *E. damarcoi*) or a highly arched anterior border with a comparatively higher process. On the contrary, in some extant individuals, the dorsal border of the acromion is straight and the anterior border may be only slightly convex. More interstingly, the coracoid process develops from a surface that is anterior to the cranial margin in the extant sperm whale but posterior in *E. damarcoi*.

The scapula is known also in some fossil sperm whales. In *Zygophyseter varolai*, the cranial margin of the scapula projects anteriorly in a notable way providing an evident expansion of the scapula along the anteroposterior axis with consequent increase of muscular attachment areas (Bianucci & Landini 2006). In this species, the acromion and the coracoid process are very close and, in medial view, it seems that the dorsal border of the coracoid process covers the view of the ventral border of the acromion. The acromion itself is elongated and its dorsal border is scarcely concave. The scapula of *Brygmophyseter shigensis* Hirota & Barnes, 1994 is highly divergent from those of *E. damarcoi* and of the extant sperm whale in that it shows a marked elongation of a narrow region of the dorsal border of the scapula in which both the anteroproximal and the posteroproximal corners protrude far more distantly than the respective cranial and caudal margins of the scapula located below them (Kimura et al. 2006). In *Brygmophyseter shigensis*, the supraspinous fossa is reduced to a degree that most of the portion close to the coracoid process is hidden by a well-raised scapular spine and only a narrow strip of the supraspinous fossa is observed in lateral view as it approaches the dorsal margin of the bone. The acromion is approximately square in shape with straight dorsal and ventral borders and cranial border slightly convex and projecting sharply anteroventrally. The coracoid process develops from a surface that is located more posterior than the cranial margin.

In the extant species of *Kogia*, the scapula is morphologically different from that of the physeteroid species described up to now. Such a scapula is comparatively longer and dorsoventrally shorter with a remarkably expanded acromion and a large coracoid process. The latter is particularly different from that of physeteroid because it is massively enlarged (Pinedo 1987).

In the extant *Physeter macrocephalus*, the humerus shows an anteriorly concave deltopectoral crest but in *Eophyseter damarcoi* the deltopectoral crest shows a straight outline. Such an outline is also exhibited by a humerus that was reported by Kimura et al. (2006) and referred to *Aulophyseter morricei*.

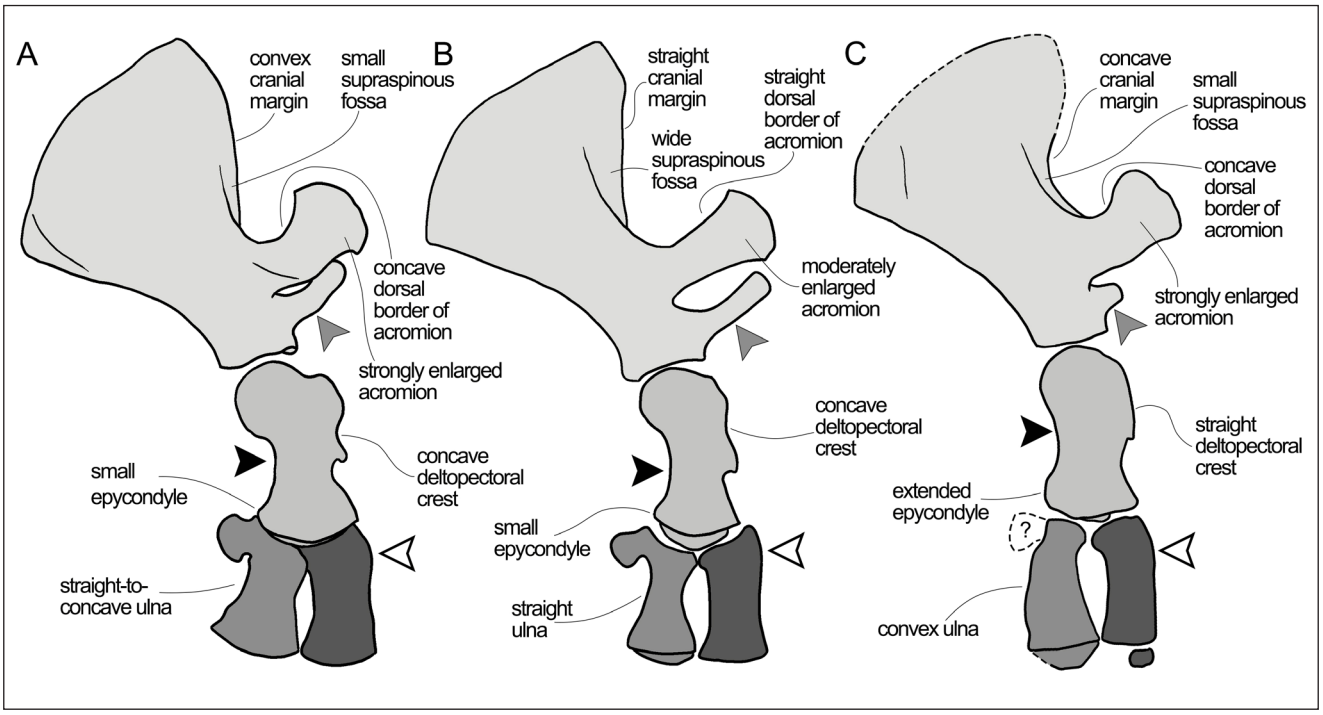

Fig. 23 - Comparative plate showing the right forelimb in the extant sperm whale, *Physeter macrocephalus*, and MGPT-PU 13864, *Eophyseter damarcoi* gen. nov. sp. nov. A) Right forelimb of *P. macrocephalus* from southern hemisphere modified from Flower (1864). B) Right forelimb of *P. macrocephalus* from northern hemisphere modified from Omura et al. (1962). C) Right forelimb of *E. damarcoi* reconstructed from the preserved bones of the holotype. Forelimbs are drawn at the same proximodistal size. Characters discussed in the text are indicated. The black arrowhead indicates the posterior border of the humerus that may be very concave, moderately concave and mostly straight. The white arrowhead indicates the relative development of the radial process. The grey arrowhead indicates the position of the basis of the coracoid process that may be at the level of or posterior to the cranial margin of the scapula.

However, in the same paper, two additional humeri were referred to the same taxon despite the presence of an anteriorly concave deltopectoral crest. A straight deltopectoral crest is also observed in *Brygmophyseter shigensis* (Kimura et al. 2006). In all these humeri and in *Eophyseter damarcoi* the posterior border of the humerus is straighter than in the extant *P. macrocephalus* (Fig. 23A-C). Interestingly, in the specimens referred to *Aulophyseter morricei* Kellogg, 1927 the distal termination of the deltopectoral crest corresponds to a protruding tubercle (= tuberculum deltoideum) resembling that of the extant sperm whale; such a tubercle is present also in *Eophyseter damarcoi* but, in this species, it projects distally rather than anteriorly. In *Kogia* the humerus shows a shorter deltopectoral crest, straight posterior border of the shaft and triangular and posteriorly-protruded posterodistal corner.

In *Eophyseter damarcoi*, the epicondyle for the olecranon process of the ulna is located more dorsal than in the extant sperm whale resembling that of *Brygmophyseter shigensis*. In the humeri referred to *Aulophyseter morricei* the epicondyle is distally positioned and the crest separating the ulnar facet from the radial facet is visibly triangular and protruding. In *B. shigensis*, *E. damarcoi* and *Physeter macrocephalus* this crest is rounded and shallow.

With respect to the extant sperm whale, *Eophyseter damarcoi* shows several different characters in the humerus: these include the straighter posterior margin of the bone, the higher epicondyle, the straight deltopectoral crest and a distally-projecting tuberculum deltoideum (Fig. 23). While the concave deltopectoral crest seems a fixed character states in sperm whales, the more or less linear outline of the posterior margin of the humerus could be due to individual variation. Again, more extensive study of the postcranial skeleton of the extant sperm whale is necessary to test this hypothesis.

The radius of *Eophyseter damarcoi* is characterized by a stocky and rectangular shape with an anterior convexity, corresponding to the radial process, that is located slightly distal from the proximal epiphysis. A possible radial process seems absent in *Brygmophyseter shigensis* based on the images published by Kimura et al. (2006) but it is present in the

unidentified sperm whale MSNUP-I 17076 from the Miocene of southern Italy as figured by Peri et al. (2020). In *Kogia* the radius is comparatively short and stocky, shows parallel and straight anterior and posterior borders and expanded and robust distal epiphysis.

The radius of *Eophyseter damarcoi* shows largely parallel anterior and posterior margins resembling the radius of *B. shigensis* but differing from that of *P. macrocephalus* in that it lacks the triangular protrusion observed at the posterodistal corner and the overall concave outline of the posterior margin (Fig. 237). As a whole, in the extant sperm whale the radius has a more robust aspect than that of *Eophyseter damarcoi* that looks more slender.

As far as the ulna is concerned, in *E. damarcoi* the posterior margin is convex and this is not observed in the extant sperm whale (Fig. 23). In the scarce ulnae reported in the sperm whale fossil record, the posterior margin of the ulna is linear in outline in MSNUP-I 17076 (Peri et al. 2020) and *Brygmophyseter shigensis* (Kimura et al. 2006). We observe that in *Physeter macrocephalus* the distal portion of the anterior margin of the ulna projects anteriorly forming a triangular protrusion which gives the bone an anteriorly concave outline (Fig. 27A, B). The olecranon is well-developed in the extant sperm whale, MSNUP-I 17076 and *Brygmophyseter shigensis* but it is lost in *Eophyseter damarcoi*. Overall, the ulna of *Physeter macrocephalus* looks more robust and stocky than that of *Eophyseter damarcoi* which is moderately more robust than MSNUP-I 17076 and comparable in proportions to that of *Brygmophyseter shigensis*. In *Kogia*, the ulna shows a reduced olecranon and slightly convex posterior border with anteroposteriorly expanded distal end.

Ribs

The articular head of the first rib of *Eophyseter damarcoi* differs from that of the sperm whale figured by Omura et al. (1962) in that the tuberculum is more slender and the capitulum shows a proximal convexity instead of a flat surface. A similar convexity, but developed at a higher degree, is observed in the first rib of *Rhaphicetus valenciae* Lambert et al., 2020 from the Early Miocene of Peru and *Zygophyseter varolai* from the Late Miocene of southern Italy (Bianucci & Landini 2008). In the latter, the tuberosity for the iliocostal muscle is well developed and triangular in the first and in the putative second rib whereas such a development is not observed in *R. valenciae* nor in *E. damarcoi*. The fragmentary ribs of *Physeterula dubusi* and MSNUP I-17076 are too poorly preserved to allow detailed comparisons (Lambert 2008; Peri et al. 2020).

In the description of the ribs of *Kogia breviceps*, Omura et al. (1954) shows that the first rib does not show the distal expansion observed in *E. damarcoi* and the internal angle is more acute than that of *E. damarcoi* and *P. macrocephalus*. Moreover, in *K. breviceps* the tuberosity for the attachment of the ileocostal muscle is triangular and well-developed in the 1st and in the 4th-to-10th ribs but it is only slightly developed and scarcely defined in *E. damarcoi*.

The distal end of the first rib of *E. damarcoi* differs from the corresponding rib observed in the extant sperm whale because its lateral corners project laterally forming a sort of rectangular expansion with concave lateral border (visible in Fig. 15, ribs *a* and *b*) that is absent in both the modern *Physeter macrocephalus* and in *Zygophyseter varolai*, the only fossil physeteroid where the first rib is entirely preserved. Rib *b* (Fig. 15) differs from all the ribs of *Physeter macrocephalus* in that it shows a higher and larger head with short tuberculum and scarcely concave proximal neck between tuberculum and capitulum. Such a rib shows a higher degree of robustness of the proximal portion even in comparison to *Zygophyseter varolai*.

Functional regionalization of the vertebral column

Conspicuous differences in the proportions of the vertebral centra are observed in *Eophyseter damarcoi* with respect to extant *Physeter macrocephalus*. Lengths of vertebral bodies increase their values along the vertebral column up to approximately vertebrae nos. 23-25 (Supplementary Information Fig. S2A). More posteriorly, the lengths abruptly diminish towards the posterior-most portion of the tail. This pattern is shared by both *Eophyseter damarcoi* and *Physeter macrocephalus*.

Widths of vertebral bodies show limited variation in the extant *Physeter macrocephalus* up to vertebrae nos. 16-18 (Supplementary Information Fig. S2B), then the widths increase up to vertebae

nos.23-25; more posteriorly the widths abruptly diminish. This pattern is not completely shared by *Eophyseter damarcoi* in that in this species the widths do not increase their value in the vertebrae Nos 16-18 and 25-26; rather, the width show very limited variation in the anterior and central portions of the vertebral column. The decrease of the widths in the posterior caudal section is not as abrupt as that observed in the living *Physeter macrocephalus*.

A similar pattern is observed in the analysis of the variation of the width of vertebral centra (Supplementary Information Fig. S2C). Also in this case, the variation of the heights in *Eophyseter damarcoi* is minimal and the heights are very similar up to vertebra no. 25 when heights sharply decrease. In *Physeter macrocephalus*, the heights gradually increase up to a plateau approximately from vertebra 12 to vertebra 27 when heights steeply decrease in the posterior portion of hte tail. These three analyses show that the outline of the vertbral centra of *Eophyseter damarcoi* is different from that observed in *Physeter macrocephalus* for a large part of the vertebral column approximately ranging from the first thoracic vertebra to vertebra 25 corresponding to Ca_6. Apart from functional interpretations, these differences can be used to distinguish *Eophyseter damarcoi* from *Physeter macrocephalus* giving the postcranial skeleton a previously unsuspected importance.

The above differences are even more evident when the above parameters of *Eophyseter damarcoi* are plotted against those of the four individuals of the extant *Physeter macrocephalus*. As shown in Supplementary Information Fig. S2A, B, widths, heights and lengths of *Eophyseter damarcoi* exhibit different relationships to each other with respect to what observed in the extant species. In particular, the most striking observation is about the existence of a region of the vertebral column where the lengths show higher values than both widths and heights in *Eophyseter damarcoi*. This pattern is never observed in *Physeter macrocephalus* where lengths are lower than heights and widths along the whole vertebral column. By means of this, the geometry of the vertebral centra of *Eophyseter damarcoi* appears largely different from that of *Physeter macrocephalus*; in *E. damarcoi* the vertebrae are comparatively longer with respect to their heights at least in a region between vertebrae 12 and 26. Following the analyses of Buchholtz (2001), comparatively longer vertebrae are related to enhanced flexibility of the vertebral column and such an increased flexibility is inferred in *Eophyseter damarcoi* with respect to *Physeter macrocephalus*.

The plot of the relative centrum length (RCL) confirms the above observation showing that a long portion of the vertebral column of *Eophyseter damarcoi* is characterized by proportionally longer vertebrae with respect to their heights and widths (Supplementary Information Fig. S4A). This region is even more evident in this plot approximately from vertebrae nos. 13 and 35 (RCL > 1). In the extant *Physeter macrocephalus*, RCL < 1 along almost all the vertebral column; RCL > 1 only in the one of the last caudal vertebrae. In Supplementary Information Fig. S4B and C, the %change values and the CW/CH ratios are shown. The %change values of *Eophyseter damarcoi* show high variation with respect to *Physeter macrocephalus*; while the distribution of the points of this parameter follow quite precisely that of the extant sperm whale, there are points falling outside the general distribution area that are difficult to interpret. The CW/CH ratios express the degree ovalization of the outline of the vertebral centra; judging from Supplementary Information Fig. S4C, the vertebrae of *Eophyseter damarcoi* show a pattern of variation of this parameter that is fully consistent with that of the extant *Physeter macrocephalus*.

Based on the above comparisons we establish the following functional regions in the vertebral columns of the extant *Physeter macrocephalus* and the fossil *Eophyseter damarcoi*: (a) the chest extends from vertebra no. 8 (T_1) to vertebra no. 11 (T_4); (b) the torso extends from T_5 to Ca_{14} or vertebra no. 36; (c) the peduncle extends from Ca_{15} (vertebra no. 37) to Ca_{20} (vertebra no. 46); (d) the fluke extends beyond Ca_{21} (vertebra no. 47). As a whole, in the vertebral column of *Physeter macrocephalus* and *Eophyseter damarcoi* the torso represents the longer portion, chest and fluke are reduced parts (Supplementary Information Fig.4). Even though the functional regions of the vertebral column have approximately the same extension in the whole sample examined, details of variation within these regions (explained above and in Figs. 28 and 29) are evident that suggest that the ways these regions worked in *Eophyseter damarcoi* were different and this, in turn, suggests a different swimming behavior for this fossil species.

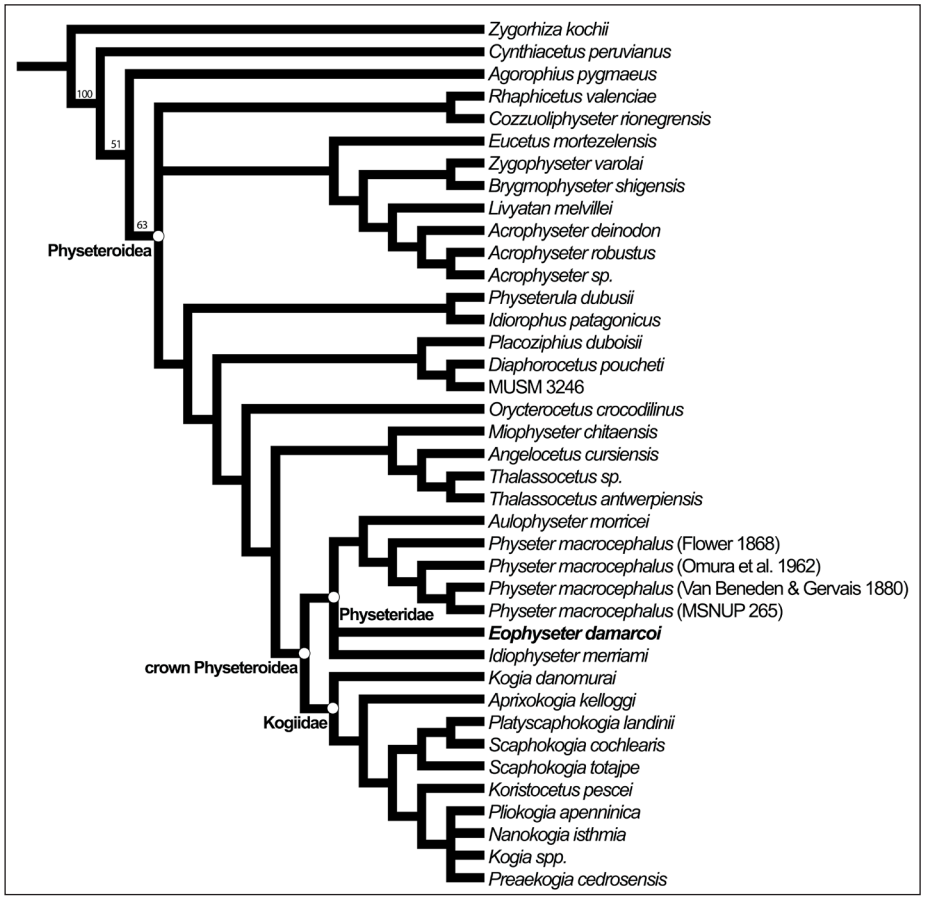

Fig. 24 - Fifty-percent, majority-rule Strict consensus (Nelsen) tree representing phylogenetic relationships of Physeteroidea. Main physeteroid clades are indicated. Numbers above the rami represent bootstrap supporting values. *Eophyseter damarcoi* gen. nov. sp. nov. is in boldface. The extant *Physeter macrocephalus* is represented by four specimens to include as much as individual variation is possible.

Phylogenetic analysis

Phylogenetic results

The TBR algorithm found six equally-parsimonious trees whose strict consensus is shown in Fig. 24. The trees are 247 steps in length and show CI = 0.514, RI = 0.714 and HI = 0.486. The strict consensus is rather well-resolved an shows that Physeteroidea is monophyletic and includes several sub-clades. The earliest-diverging physeteroid include *Rhaphicetus* and *Cozzuoliphyseter*. The subsequent clade includes the so-called killer sperm whales and their sister group represented by *Eucetus mortezelensis*. This clade is the sister group of another large clade including a series of sub-clades represented by *Physeterula*+*Idiorophus*, *Placoziphius*+*Diaphorocetus*+MUSM 3246, and a group formed by *Orycterocetus*, *Kogia*, their common ancestor and all the descendants of this ancestor. In particular, this large group includes a clade formed by *Angelocetus*+*Thalassocetus*+*Miophyseter* that is the sister group of the crown Physeteroidea including Kogiidae and Physeteridae. Physeteridae is formed by *Idiophyseter*, *Eophyseter*, *Aulophyseter* and *Physeter*. The sister group of the living *Physeter macrocephalus* is identified in *Aulophyseter morricei* and *Idiophyseter* and *Eophyseter* occupy basal and unresolved positions in this clade.

Bootstrap supporting values are low as expected judging from the results using the previously published part of the present dataset. The monophyly of Physeteroidea is well-supported by bootstrap but the other clades received bootstrap supporting values lower than 50%.

Synapomorphy reconstructions at selected nodes

We analyzed the distribution of characters 59-78 at the internal nodes of the strict consensus tree by the maximum likelihood (ML) algorithm as implemented in Mesquite and found that most of these characters can be used to respectively diagnosize Physeteridae and *Physeter* as these have ML values higher than 0.8. The results of this analysis are shown in Table 6. Interstingly, we found that the postcranial skeleton may be an important source of morphological data able to support a higher resolution of the phylogenetic results. In particular, our analysis suggests that a robust radius (in the sense

Clade	Character No. (state)	Character description	ML
Physeteridae	60(1)	*Inferior portion of neural canal of atlas: narrow*	0.55
	65(1)	*Posterior epiphysis of axis-bearing block (C_7): wide (height/width ratio equals* c. *0.45)*	0.88
	69(1)	*Superior border of acromion: mostly concave*	0.75
	72(1)	*Anterior projection of the distal epiphysis of humerus: large*	0.87
	75(1)	*Radius robustness: robust (proximodistal/anteroposterior diameters < 2.5)*	0.99
	78(1)	*Outline of capitulum in first rib: convex*	0.83
Physeter	59(2)	*Neural spine of atlas: absent*	0.64
	61(1)	*Neural arch of the atlas: linear*	0.56
	64(1)	*Width of axis in anterior view: wide (height/width ratio equals* c. *0.5)*	0.92
	68(1)	*Extent of supraspinous fossa of scapula: narrow (angle between cranial margin and scapular spine < 30°)*	0.91
	71(1)	*Relative height of the ulnar epicondyle of humerus: close to the ulnar articular facet*	0.99
	73(1)	*Shape of deltopectoral crest of humerus: anteriorly concave*	0.99
	74(1)	*Anterior protrusion of deltoid tubercle of humerus: present*	0.99
	76(1)	*Radial process: reduced to a radial crest*	0.99

Tab. 6 - Synapomorphies of postcranial skeleton supporting Physeteridae and *Physeter*. Numbers represent maximum likelihood probabilities (ML) reconstructed by MESQUITE.

specified in Supplementary Information Text S1, character 75), a large anterior protrusion of the distal epiphysis of the humerus (character 72), and a wide posterior epiphysis of the axis-bearing block (in the sense specified in Supplementary Information Text S1, character 65) may be considered as synapomorphic for Physeteridae with a good degree of likelihood (> 0.85).

The monophyly of *Physeter* is based on the following synapomorphies with ML values > 0.85: wide axis in anterior view (character 64), narrow supraspinous fossa (character 68), ulnar epicondyle close to the articular facet for ulna (character 71), anteriorly concave deltopectoral crest of humerus (character 73), presence of anterior protrusion of the deltoid tubercle (character 74), and radial process reduced to a crest (character 76). None of these characters have ML value = 1 and this means that convergent evolution of some of them can be observed in other physeteroid clades. However, the high ML value observed suggest that these character states are plesiomorphic for *Physeter* and the variation observed today may be attributed to secondary reversals to ancestral states or relaxed selection for given morphological character states at particular districts.

Discussion

Postcranial skeleton and cetacean systematics

Postcranial skeletons are often neglected in cetacean paleontology and systematics. It is a common practice to make diagnoses of new cetacean taxa based on characters observed in the skull and the ear bones, including periotic and tympanic bulla. In some cases, the ear bone characteristics are prevailing over the other cranial and postcranial districts as far as characters that can be used in phylogenetic analyses (e.g., Tanaka & Fordyce 2016; Tsai & Fordyce 2016;). This practice is historically-based on works about basicrania of a number of mammalian clades and relies on the idea that this part of the skull exhibits a high degree of complexity because it is related to the paths of several cranial nerves and brain vasculature; such a complexity offers the possibility to identify many potentially-informative morphological characters (e.g., Luo & Gingerich 1999; Novacek 1993, 1986). While reasonable, this assumption does not preclude the possibility that also other parts of the whole body of the specimens under investigation may include unique, e.g. diagnostic, morphological characters that can be used to unambiguously distinguish them from all the other members of their supraspecific group. According to diagnosis definitions proposed by Mayr (1969), Wiley (1981) and Dubois (2017) as reviewed by Borkent (2021), all the morphological characters can be used to establish a diagnosis of a new species or genus or other suprageneric taxon.

Recently, a detailed morphological investigation revealed the presence of unique character states in the postcranial skeleton of a Pliocene balaenid from Reggio Emilia so that it was possible to distinguish that specimen from all the other balaenid cetaceans described up to now, and assign

it to the new genus and species *Charadrobalaena valentinae* (Bisconti et al. 2023b). The same applies in the present analysis of the postcranial skeleton of the Pliocene sperm whale MGPT-PU 13864. In the lack of skull and ear bones, the detailed analysis of the shapes of the vertebrae and of the outlines of the vertebral bodies, together with an in-depth study of both humerus and ulna, revealed unique morphologies that unambiguously distinguish this specimen from all the other extant and fossil sperm whale species described up to now. In the present case, the vertebrae differ from those of other sperm whales in the relative roundness of the outline of the centra and in the proportions of lengths, heights and widths of the vertebral bodies. The differences are presented in Supplementary Information Figs S2-4 and explained in the section titled Functional regionalization of the vertebral column. Based on these distinguishing characters of the vertebrae and on the peculiar morphologies of the deltoid crest and of the posterior convexity of the ulnar shaft, we decided to unambiguously identify this combination of morphological characters as the new genus and species *Eophyseter damarcoi*.

Unfortunately, only a handful postcrania are available for fossil sperm whale species in the literature and this limits the possibilities to perform extended comparisons. However, comparisons with the available materials revealed morphological differences that still enable the recognition of *Eophyseter damarcoi* as a different sperm whale taxonomic entity.

It is doubtless that higher importance has to be given to the postcranial skeleton in cetacean paleontology. While it is certainly true that skull and ear bones exhibit most of the morphological characters useful for phylogenetic analyses and taxonomic diagnoses, the postcranial skeleton has recently revealed an unsuspected morphological diversity that may be of great help in distinguishing between different taxa in the cetacean fossil record. It is to be taken in mind that some high-rank cetacean taxa have been defined based in part or completely on postcranial characters; these include, for instance, Neoceti (e.g., Boessenecker et al. 2020), Pachycetinae (Gingerich et al. 2022) and some archaeocete genera (e.g., Gingerich 2007, 1997). Moreover, the postcranial skeleton is related to the biomechanics of movements such as swimming in whales and can provide researchers with information about ecology and behaviors of fossil species (e.g., Buchholtz 2001). We recommend that future studies include detailed analyses of the postcranial skeleton of fossil whales in order to allow increased comparisons for a better understanding of past diversity and ecology of whales and dolphins.

The sperm whale fauna from the Pliocene of Piedmont

Fossil sperm whales are known from the Pliocene Sabbie d'Asti Formation of Piedmont. Portis (1885) described two specimens; one corresponds to *Hoplocetus minor* Portis, 1885, a specimen previously collected by the Abbott Sotteri and subsequently acquired by Sismonda, and the other corresponds to *Physotherium sotterii* Portis, 1885, a specimen included in the Gastaldi collection before becoming part of the MGPT collection (see Bisconti & Damarco 2022; Bisconti et al. 2023a, 2020 for the reconstruction of the history of the discoveries). These specimens (respectively corresponding to specimens No. 13862 and 13863 of the collection of the Geological and Palaeontological Museum of the University of Torino) are only represented by partial dentitions and are fully figured by Bisconti et al. (2023a). The recent revision of fossil sperm whale teeth performed by Hampe (2006) did not include all the teeth represented in the Pliocene record of Piedmont because, at the times, only a few of them were available for study. However, these teeth represent evidence of sperm whale presence and diversity in the Pliocene of Piedmont.

Unfortunately, both *Physotherium sotterii* and *Hoplocetus minor* are represented by dental material only and cannot be compared to the postcranial skeleton of *Eophyseter damarcoi* and show enough differences to be assigned to different taxa by Hampe (2006).

Additionally, in one of the skeletons (MGPT-PU 13868) that was assigned to *Berardiopsis pliocaenus* by Portis (1885), the metapophyses are placed at a comparatively high position in the lateral sides of the neural arch differing from those of ziphiids and resembling those of Physeteridae; this is clearly shown in Bisconti et al. (2023a) plate 70b. Vertebral size precludes the inclusion of this skeleton within the known sperm whale species, including *E. damarcoi*. A partial skull was also found in close association with this skeleton but it was never prepared. Recently, the skull was CT-scanned and the availabil-

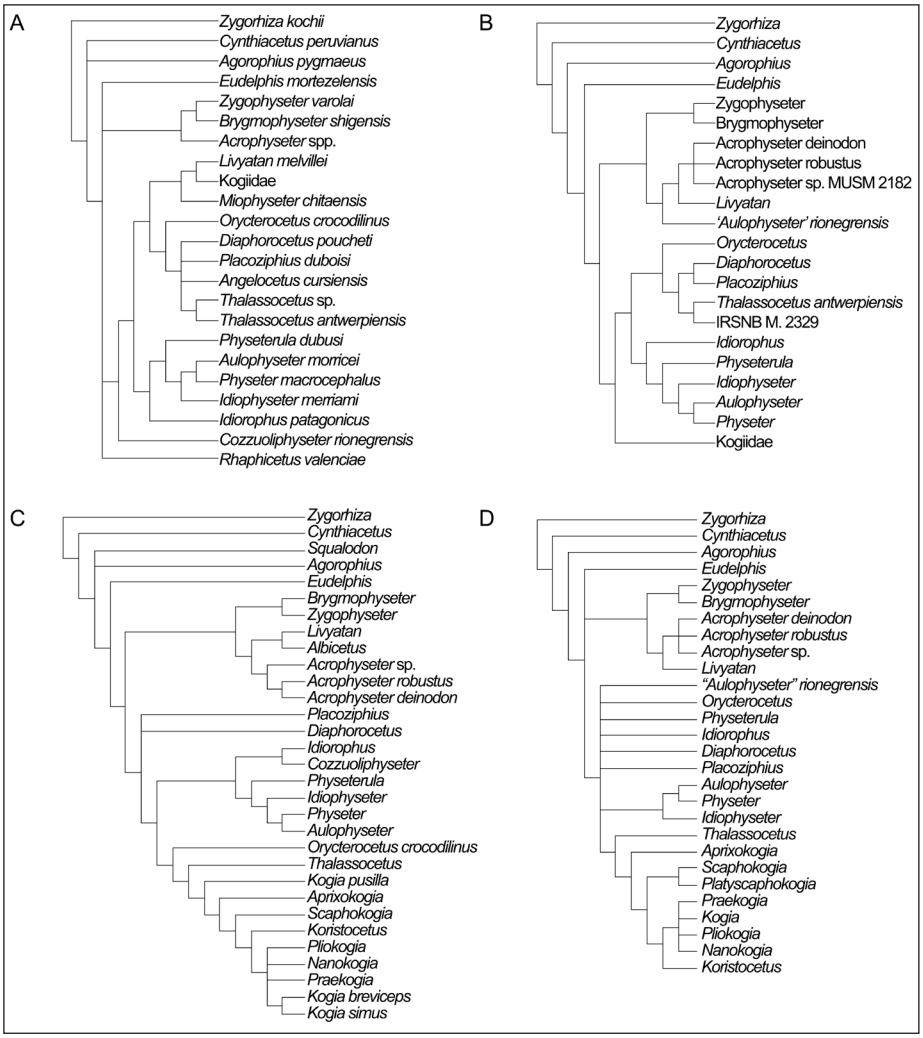

Fig. 25 - Previously published phylogenetic hypotheses for Physeteroidea relationships. A, redrawn from Peri et al. (2022). B, redrawn from Alfsen et al. (2021). C, redrawn from Paolucci et al. (2020, traditional search, unordered characters, implied weights). D, redrawn from Collareta et al. (2020).

ity of the new images will allow its full analysis and characterization. As *Berardiopsis* was discovered in the Asti province, it represents further evidence of another potential physeteroid taxon in the Pliocene of Piedmont. The full analysis of all this material will require some time and is currently in progress.

Phylogenetic remarks

Our anatomical work shows that the postcranial diversity of the physeteroid skeletons should be taken into account when trying to describe the phylogenetic history of this group. The postcranial skeleton shows a wealth of different morphologies that may be interpreted in both functional and evolutionary terms as they may give insights about the evolutionary patterns exhibited by extant and fossil sperm whales and the origin of the adaptations of extant *Physeter* to the extreme *habitat* that it exploits. Unfortunately, the postcranial remains of extinct sperm whale species are rare and for this reason all previously published phylogenetic analyses of sperm whales relied on the morphology of the skull and ear bones. In any case, the use of cranial characters was not enough to obtain well-resolved phylogenetic results; the most recent works, indeed, resulted in cladograms in which traditionally recognized physeteroids are variously subdivided into several branches in an unresolved polytomy (Fig. 25). This is observed in the results of Peri et al. (2022), for instance (Fig. 25A). In that paper, *Rhaphicetus* and *Acrophyseter+Zygophyseter+Brygmophyseter* represent two separate clades that emerge from an unresolved polytomy including also a large crown physeteroid clade that, in turn, comprises *Livyatan*, modern physeterids and kogiids. Interestingly, in that result, *Livyatan* is the sister group of Kogiidae; Physeteridae includes *Physeterula+Idiorophus+Idiophyseter+Aulophyseter* and *Physeter*.

Alfsen et al. (2021) found the group including *Idiorophus+Idiophyseter+Aulophyseter+Physeter*, and well-resolved groupings for the other physeteroid clades (Fig. 25B). Collareta et al. (2019, 2020) and

Benites-Palomino et al. (2020) found alternative solutions (Fig. 25D); the results of the latter suggested that *Physeter* is not closely related to *Idiorophus*.

The morphological support to the clades individuated in the previous phylogenetic analyses of sperm whales is low; this is shown by the bootstrap supporting values published in the papers published up to now and in the present work. Interestingly, Paolucci et al. (2020) concluded through their analysis that *Diaphorocetus* sp. was particularly unstable because of poor preservation and homoplastic distribution of character states (Fig. 25C). The instability of taxa across the cladograms is an important problem for morphology-based phylogenetic analyses of sperm whales and probably requires more in-depth anatomical analysis of extant and fossil physeteroids to be resolved.

Our inclusion of 20 new morphological characters to the dataset certainly increases the morphological sample together with our inclusion of four specimens of the extant *Physeter macrocephalus* (increasing both morphological and taxonomic samples) was able to ameliorate the results. In fact, all this new evidence resulted in what is probably the strict consensus tree characterized by the highest resolution ever published up to now. The present results are thus based on both increased taxonomic and morphological samples including the usually neglected postcranial skeleton even in the presence of some degree of individual variation.

The functional regionalization of the vertebral column of *Eophyseter damarcoi* represents a clear example of such a diversity in that it shows, for the first time, that the functional regions of the vertebral column of an extinct sperm whale exhibit morphometric and morphological differences with respect to the extant *Physeter macrocephalus*. This suggests that aspects of the swimming biomechanics and behavior evolved differently in these two sperm whale lineages. Our analyses show that the main vertebral differences between *Eophyseter damarcoi* and *Physeter macrocephalus* are in the relationships between length of the centra and height and width. According to Buchholtz (2001 and literature therein), these differences are related to differences in swimming behavior because long centrum lengths are associated to column flexibility. As the relative centrum length values of *Eophyseter damarcoi* are comparatively higher than those of the extant sperm whale specimens, we predict a higher flexibility of the torso in *E. damarcoi*. In *E. damarcoi* we observe that the values of the relative centrum length of the peduncle and fluke approximate those of the extant sperm whale specimens suggesting similar decrease in column flexibility. Therefore, we expect that in the swimming of *Eophyseter damarcoi*, most of the torso was able to exhibit a higher dorsoventral undulation than the modern *P. macrocephalus* but in both species the peduncle and fluke had very similar functional performances.

These inferred differences highlight unsuspected functional diversity in the lineage leading to the extant *Physeter macrocephalus*. This strongly suggests that postcranial skeletons of fossil sperm whales have to be carefully collected and studied in order to better understand the evolution of physeteroid diversity, relationships and ecology.

Conclusions

We report the discovery of a new sperm whale genus and species, *Eophyseter damarcoi*, from the early Piacenzian of Piedmont, northwest Italy. The holotype skeleton consists of a partially articulated vertebral column, ribs, three chevrons and portions of both forelimbs.

Measurements of the vertebrae revealed that *Eophyseter damarcoi* possessed a vertebral column profoundly different from that of its extant relative, *Physeter macrocephalus*; such a vertebral column is characterized by more elongated vertebral centra that suggest different swimming abilities with respect to the extant *P. macrocephalus* (following the suggestions made by Buchholtz, 2001 about the correlation between height:width:length rations of vertebral centra in extant and extinct cetaceans). The robustness of the proximal portions of the ribs corroborates this conclusion because it is related to the expansion of the attachment sites for axial musculature active during the generation of the stroke in the swimming and shows conspicuous differences with the extant sperm whale species.

Morphologically, *Eophyseter damarcoi* differs from the extant *P. macrocephalus* in details in the atlas, axis, scapula, humerus and ulna. In particular, the lower robustness of radius and ulna is a striking difference with the extant sperm whale species. Our comparative analysis reveals morphological variation between the northern and southern populations of the extant sperm whales.

From a phylogenetic point of view, our results show that the morphological support for phylogenetic relationships among Physeteroidea greatly benefits from adding more extended taxonomic and morphological samples even in the presence of a certain degree of individual variation. Our analysis resulted in a better resolved strict consensus cladogram than those previously published. Our results confirm the placement of *Eophyseter damarcoi* within Physeteridae and the sister group relationship of *Aulophyseter* and *Physeter*.

Data Availability Statement

The data supporting the results of this research are available upon request. Interested researchers may contact the corresponding author to obtain access.

Acknowledgements: Many thanks are due to all those students who assisted in the preparation of the Vigliano sperm whale whose names are as follows: Francesca Busa, Riccardo Daniello, Andrea Fragomeni, Alexandra Savescu, Riccardo Stecca. Piero Damarco coordinated the preparation of the specimen and prepared himself parts of it; he kindly provided images for Figs 9-14 and 16 together with measurements of chevrons and sternum, and bibliographic data. Many thanks are due to Olivier Lambert and an another anonymous referee for their constructive comments that helped to increase clarity and scientific content of this paper. Many thanks are also due to Marta Zunino and to the Soprintendenza Archeologia Belle Arti e Paesaggio per le Province di Alessandria, Asti e Cuneo for the authorization to study the Vigliano sperm whale (authorization Prot. No. 10580, July, 24th, 2024). In this paper, RS provided bibliographic data; RD realized the photogrammetry and wrote the corresponding methodological section; MB studied and measured the specimen, performed the comparative, biomechanic and phylogenetic analyses, and wrote the paper; GC coordinated the research group; all the authors commented on the manuscript. This research was funded by University of Torino ex-60% Funds to GC and funds from the MPTA.

References

Abel O. (1905) - Odontocètes du Boldérien (Miocène Supérieur) d'Anvers. *Memoires du Musée Royal d'Histoire Naturelle de Belgique*, 3: 7-155.

Alfsen A., Bosselaers M. & Lambert O. (2021) - New sperm whale remains from the late Miocene of the North Sea and a revised family attribution for the small crown physeteroid *Thalassocetus* Abel, 1905. *Comptes Rendus Palevol*, 20: 807-822.

Benke H. (1993) - Investigations on the osteology and the functional morphology of the flipper of whales and dolphins (Cetacea). *Investigations on Cetacea*, 24: 9-252.

Benites-Palomino A., Vélez-Juarbe J., Salas-Gismondi R. & Urbina M. (2020) - *Scaphokogia totajpe*, sp. nov., a new bulky-faced pygmy sperm whale (Kogiidae) from the late Miocene of Peru. *Journal of Vertebrate Paleontology*, 39: 6.

Bianucci G. & Landini W. (2006) - Killer sperm whale: a new basal physeteroid (Mammalia, Cetacea) from the Late Miocene of Italy. *Zoological Journal of the Linnean Society*, 148: 103-

Bisconti M. & Carnevale G. (2022) - Skeletal Transformations and the Origin of Baleen Whales (Mammalia, Cetacea, Mysticeti): A Study on Evolutionary Patterns. *Diversity*, 14, 221.

Bisconti M. & Damarco P. (2022) - The paleontological and cultural heritage of the fossil cetaceans from the Pliocene of Valleandona. In Marramà G. & Carnevale G., eds. *Volume dei Riassunti e Guida all'Escursione. Paleodays 2022 – XXII Edizione delle Giornate di Paleontologia*. Museo Regionale di Scienze Naturali e Società Paleontologica Italiana, Torino: 167-186.

Bisconti M., Damarco P., Repetto G., Pavia M. & Carnevale G. (2020). - Il patrimonio paleocetologico piemontese: storia e prospettive. In Francou C., ed. *Pliocenica 2020 – I cetacei tornano a Castell'Arquato – Italian paleocetology reviews*. *Parva Naturalia*, 15: 15-58.

Bisconti M., Damarco P., Pavia M., Sorce B. & Carnevale G. (2021a) - *Marzanoptera tersillae*, a new balaenopterid genus and species from the Pliocene of Piedmont, north-west Italy. *Zoological Journal of the Linnean Society*, 192: 1253-1292.

Bisconti M., Damarco P., Carnevale G. & Pavia M. (2021b) - I cetacei fossili della Valle Andona. In Berzano L., Damarco P., Pavia G., Bisconti M., Sarti C., Monetti Giambrone L. & Fassio A., eds. *Valle Andona mare e fossili*. Elledici, Torino: 175-203.

Bisconti M., Damarco P., Santagati P., Pavia M., Carnevale G. (2021c) - Taphonomic patterns in the fossil record of baleen whales from the Pliocene of Piedmont, North-West Italy (Mammalia, Cetacea, Mysticeti). *Bollettino della Società Paleontologica Italiana*, 60: 183-211. Doi:10.4435/BSPI.2021.14

Bisconti M., Damarco P., Pavia M. & Carnevale G. (2023a) - *Catalogo illustrato dei mammiferi marini fossili dei musei piemontesi*. Elledici, Torino, 352 p.

Bisconti M., Chicchi S., Monegatti P., Scacchetti M., Campanini R., Marsili S. & Carnevale G. (2023b) - Taphonomy, osteology and functional morphology of a partially articulated skeleton of an archaic Pliocene right whale from Emilia Romagna (NW Italy). *Bollettino della Società Paleontologica Italiana*, 62: 1-32.

Boessenecker R.W. (2013) - A new marine vertebrate assemblage from the late Neogene Purisima Formation in Central California, part II: Pinnipeds and Cetaceans. *Geodiversitas*, 35: 815-940.

Borkent A. (2021) - Diagnosing diagnoses – can we improve our taxonomy? *ZooKeys*, 1071: 43-48.

Brisson A.D. (1762) - *Regnum animale in classes IX Distributum, sive synopsis methodica. Lugdum Batarorum, apud*. Theodorum Haak, Leiden, 384 p.

Buchholtz E.A. (1998) - Implications of vertebral morphology for locomotor evolution in early Cetacea. In Thewissen J.G.M., ed. *The Emergence of Whales*. Plenum Press, New York: 325–351.

Buchholtz E.A. (2001) - Vertebral osteology and swimming style in living and fossil whales (Order: Cetacea). *Zoological Journal of the Linnean Society*, 253: 175-190.

Buchholtz E.A. & Schur S.A. (2004) - Vertebral osteology in Delphinidae (Cetacea). *Zoological Journal of the Linnean Society*, 140: 383-401.

Buchholtz E.A., Wokovich E.M. & Cleary R.J. (2005) -

Vertebral osteology and complexity in *Lagenorhynchus acutus* (Delphinidae) with comparison to other delphinoid genera. *Marine Mammal Science*, 21: 411-428.

Collareta A., Cigala Fulgosi F. & Bianucci G. (2019) - A new kogiid sperm whale from northern Italy supports psychrospheric conditions in the early Pliocene Mediterranean Sea. *Acta Palaeontologica Polonica*, 64: 609-626.

Collareta A., Lambert O., Muizon C. de, Benites Palomino A. M., Urbina M. & Bianucci G. (2020) - A new physeteroid from the late Miocene of Peru expands the diversity of extinct dwarf and pygmy sperm whales (Cetacea: Odontoceti: Kogiidae). *Comptes Rendus Palevol*, 19: 79-100.

Damarco P. (2009) - La formazione di un territorio-Storia geopaleontologica dell'Astigiano. *Quaderni Scientifici dell'Ente Parchi Astigiani*, 7: 1-312.

Damarco P., Fassio A., Imbriano F., Delmastro G. & Bisconti M. (2023) - La mostra sui cetacei fossili piemontesi al Museo dei Fossili di Asti. *GeologicaMente*, 10: 62-63.

Dubois A. (2017) - Diagnoses in zoological taxonomy and nomenclature. *Bionomina*, 12: 63-85.

Du Bus B.A.L. (1872) - Mammifères nouveaux du Crag d'Anvers. *Bulletin de l'Académie Royale des Sciences, des Lettres et des Beaux-Arts de Belgique*, 34: 491-509.

Flower W.H. (1867) - On the osteology of the cachalot or sperm-whale (*Physeter macrocephalus*). *Transactions of the Zoological Society of London*, 6: 309-372.

Flower W.H. (1868) - On the osteology of the cachalot or sperm-whale (*Physeter macrocephalus*). *Journal of Zoology*, 6: 309-372.

Fordyce R.E. & Muizon C. de (2001) - Evolutionary history of whales: a review, *in* Mazin J.-M. & Buffrenil V. de (eds.), *Secondary adaptation of tetrapods to life in water. Proceedings of the international meeting*. Verlag Dr Friedriech Pfeil, München: 169-234.

Gingerich P.D., Amane A. & Zouhri S. (2022) - Skull and partial skeleton of a new pachycetine genus (Cetacea, Basilosauridae) from the Aridal Formation, Bartonian middle Eocene, of southwestern Morocco. *PLoS ONE*, 17(10): e0276110. https://doi.org/10.1371/journal.pone.0276110.

Gingerich P.D. (2007) - *Stromerius nidensis*, new archaeocete (Mammalia, Cetacea) from the Upper Eocene Qasr el-Sagha Formation, Fayum, Egypt. *Contributions from the Museum of Paleontology, University of Michigan*, 31: 363-378.

Gingerich P.D., Arif M., Bhatti M.A., Anwar M. & Sanders W.J. (1997) - *Basilosaurus drazindai* and *Basiloterus hussaini*, new Archaeoceti (Mammalia, Cetacea) from the Middle Eocene Drazinda Formation, with a revised interpretation of ages of whale-bearing strata in the Kirthar Group of the Sulaiman Range, Punjab (Pakistan). *Contributions from the Museum of Paleontology, The University of Michigan*, 30: 55-81.

Goloboff P.A. & Catalano S.A. (2016) - TNT version 1. 5, including a full implementation of phylogenetic morphometrics. *Cladistics*, 32: 231-238.

Gray J.E. (1821) - On the natural arrangement of vertebrose animals. *London Medical Repository*, 15: 296-310.

Gray J.E. (1846) - On the British Cetacea. *Annals and Magazine of Natural History*, 17: 82-85.

Hammer Ø., Harper D.A.T. & Ryan P.D. (2001) - PAST: paleontological statistics software package for education and data analysis. *Palaeontologia Electronica*, 4: 4.

Hampe O. (2006) - Middle/late Miocene hoplocetine sperm whale remains (Odontoceti: Physeteridae) of North Germany with an emended classification of the Hoplocetinae. *Fossil Record*, 9: 61-86.

Häussermann V., Gutstein C.S., Bedington M., Cassis D., Olavarria C., Dale A.C., Valenzuela-Toro A.M., Perez-Alvarez M.J., Sepúlveda H.H., McConnell K.M., Horwitz F.E. & Försterra G. (2017) - Largest baleen whale mass mortality during strong El Niño event is likely related to harmful toxic algal bloom. *PeerJ*, 5: e3123.

Kellogg R. (1927) - Study of the skull of a fossil sperm whale from the Temblor Miocene of southern California. *Publications of the Carnegie Institution of Washington*, 346: 1-23.

Kellogg R. (1936) - A review of the Archaeoceti. *Carnegie Institution Washington* 482: 1-366.

Kimura T., Hasegawa Y. & Barnes L.G. (2006) - Fossil sperm whales (Cetacea, Physeteridae) from Gunma and Ibaraki prefectures, Japan; with observations on the Miocene fossil sperm whale *Scaldicetus shigenis* Hirota and Barnes, 1995. *Bulletin of the Gunma Museum of Natural History*, 10: 1-23.

Lambert O. (2008) - Sperm whales from the Miocene of the North Sea: a re-appraisal. *Bulletin de l'Institut royal des Sciences naturelles de Belgique, Sciences de la Terre*, 78: 277-316.

Lambert O., de Muizon C., Urbina M. & Bianucci G. (2020) - A new longirostrine sperm whale (Cetacea, Physeteroidea) from the lower Miocene of the Pisco Basin (southern coast of Peru), *Journal of Systematic Palaeontology*, 18: 1707-1742.

Lambert O., Collareta A., Benites-Palomino A., Merella M., Muizon C. de, Bennion R., Urbina M. & Bianucci G. (2023) - A new platyrostrine sperm whale from the Early Miocene of the southeastern Pacific (East Pisco Basin, Peru) supports affinities with the southwestern Atlantic cetacean fauna. *Geodiversitas*, 45: 659-679.

Liebig P.M., Taylor T.-S.A. & Flessa K.W. (2003) - Bones on the beach: marine mammal taphonomy of the Colorado Delta, Mexico. *Palaios*, 18: 168-175.

Linnaeus C. (1758) - *Systema Naturae*. Salvii, Holmiae, Stockholm, 824 p.

Luo Z. & Gingerich P.D. (1999) - Terrestrian Mesonychia to aquatic Cetacea: transformation of he basicranium and evolution of hearing in whales. *University of Michigan Papers in Paleontology*, 11: 1-98.

Maddison W. & Maddison D. (2019) - *Mesquite 3.61: a modular system for evolutionary analysis*. Available at: https://www.mesquiteproject.org/

Martínez-Cáceres M., Lambert O. & Muizon C. de (2017) - The anatomy and phylogenetic affinities of *Cynthiacetus peruvianus*, a large *Dorudon*-like basilosaurid (Cetacea, Mammalia) from the late Eocene of Peru. *Geodiversitas*, 39: 7-163.

Mayr E. (1969) - *Principles of Systematic Zoology*. McGraw Hill, New York and London, 428 pp.

Nishiwaki M., Hibiya T. & Kimura S. (1956) - On the sexual maturity of the sperm whale (*Physeter catodon*) found in the North Pacific. *Scientific Reports of the Whale Research Institute*, 11: 39-46.

Nosenzo L. (2022) - *Fossili e territori. Scoperta straordinarie sulle colline astigiane*. arabA Fenice, Cuneo, 170 p.

Novacek M.J. (1993) - Patterns of diversity in the mammalian skull. In: Hanken J. & Hall B.K. eds., *The Skull: Patterns of Structural and Systematic Diversity, Volume 2*. University

of Chicago Press, Chicago: 438-529.

Novacek M.J. (1986) - The skull of leptictid insectivorans and the higher-level classification of eutherian mammals. *Bulletin of the American Museum of Natural History*, 183: 1-112.

Omura H., Nishiwaki M., Ichihara T. & Kasuya T. (1962) - Osteological note of a sperm whale. *Scientific Reports of the Whale Research Institute*, 16: 35-45.

Omura H., Shirakihara M. & Haruka I. (1984) - A pygmy sperm whale accidentally taken by drift net in the North Pacific. *Scientific Reports of the Whale Research Institute*, 35: 183-193.

Paolucci F., Buono M.R., Fernández M.S., Marx F.G. & Cuitiño J.I. (2020) - *Diaphorocetus poucheti* (Cetacea, Odontoceti, Physeteroidea) from Patagonia, Argentina: one of the earliest sperm whales. *Journal of Systematic Palaeontology*, 18: 335-355.

Paolucci F., Fernández M.S., Buono M.R. & Cuitiño J.I. (2021). - '*Aulophyseter*' *rionegrensis* (Cetacea: Odontoceti: Physeteroidea) from the Miocene of Patagonia (Argentina): a reappraisal. *Zoological Journal of the Linnean Society*, 192: 1293-1322.

Parona C.F. (1930) - Resti di un *"Physeter"* scoperti nel Pliocene (Astiano) di Vigliano d'Asti, in frazione Val Montasca. *Atti della Reale Accademia delle Scienze di Torino*, 65: 240-245.

Peri E., Collareta A. & Bianucci G. (2020). - A new record of Physeteroidea from the Upper Miocene of the Pietra leccese (southern Italy): systematics, paleoecology and taphonomy of a fossil macroraptorial sperm whale. *Rivista Italiana di Paleontologia e Stratigrafia*, 126: 751-769.

Peri E., Collareta A., Aringhieri G., Caramella D., Foresi L. M. & Bianucci G. (2022) - CT imaging, retrodeformation, systematics and paleobiology of a sperm whale from the Pietra leccese. *Bollettino della Società Paleontologica Italiana*, 61: 187-206.

Peters A.M.M. & Monteiro H.J. (2005) - A small sperm whale (Cetacea: Odontoceti, Physeteridae) from the Miocene of Antwerp. *Deinsea*, 11: 87-101.

Pinedo M.C. (1987) - First record of a dwarf sperm whale from southwest Atlantic, with reference to osteology, food habits and reproduction. *Scientific Reports of the Whale Research Institute*, 38: 171-186.

Portis A. (1884) - Catalogo descrittivo dei Talassoterii rinvenuti nei terreni terziari del Piemonte e della Liguria. *Memorie della Reale Accademia delle Scienze di Torino*, 37: 247-365.

Richard C. (1930) - Di una particolare asimmetria dei fiseteridi (asimmetria emapofisaria) e delle sue relazioni con l'asimmetria cranica. *Rendiconti della Reale Accademia Nazionale dei Lincei*, 12: 165-172.

Roselli A., Borzatti von Löwenstern A., Bisconti M. (2014) - La collezione osteologica di cetacei del Museo di Storia Naturale del Mediterraneo della Provincia di Livorno. *Museologia Scientifica Memorie*, 12: 239-248.

Sacco F. (1893) - Sopra un cranio di *Tursiops cortesii* (Desm.) var. *astensis* Sacc. dell'Astigiana. *Atti della Reale Accademia delle Scienze di Torino*, 26: 703-712.

Sacco F. (1891) - Il delfino pliocenico di Camerano Casasco. *Memorie della Società Italiana delle Scienze*, 9: 1-14.

Stecca R. (2021) - *Analisi preliminare del capodoglio pliocenico di Vigliano d'Asti*. MS thesis, University of Turin, 42 p.

Tanaka Y. & Fordyce R.E. (2016) - *Papahu*-like fossil dolphin from Kaikoura, New Zealand, helps to fill the Early Miocene gap in the history of Odontoceti. *New Zealand Journal of Geology and Geophysics*, 59: 551-567.

Tsai C.H. & Fordyce R.E. (2016) - Archaic baleen whale from the Kokoamu Greensand: earbones distinguish a new late Oligocene mysticete (Cetacea: Mysticeti) from New Zealand. *Journal of the Royal Society of New Zealand*, 46: 117-138.

Van Beneden P.-J. (1869) - Sur un nouveau genre de ziphioide fossile (*Placoziphius*), trouvé à Edeghem, près d'Anvers. *Mémoires de l'Académie Royale des Sciences, des Lettres et des Beaux-Arts de Belgique*, 37: 1-12.

Van Beneden P.-J. (1877) - Note sur un Cachalot nain du crag d'Anvers (*Physeterula dubusii*). *Bulletin de l'Académie Royale des Sciences, des Lettres et des Beaux-Arts de Belgique*, 44: 851-856.

Van Beneden P.-J. & Gervais P. (1880) - *Ostéographie des cétacés vivants et fossils*. Arthus Bertrand, Paris, 634 p.

Wiley E.O. (1981) - *Phylogenetics, the theory and practice of phylogenetic systematics*. Wiley & Sons, New York, 439 p.